(12)

DNA-TR-81-158

NUCLEAR-INDUCED LIGHTNING AURORA EXPERIMENT

J. W. Erler
B. C. Passenheim
W. G. Vulliet
V. A. J. van Lint
Mission Research Corporation
5434 Ruffin Road
San Diego, California 92123

11 August 1982

Technical Report

CONTRACT No. DNA 001-81-C-0151

APPROVED FOR PUBLIC RELEASE;
DISTRIBUTION UNLIMITED.

THIS WORK WAS SPONSORED BY THE DEFENSE NUCLEAR AGENCY
UNDER RDT&E RMSS CODE B323081466 X99QAXVC00002 H2590D.

Prepared for
Director
DEFENSE NUCLEAR AGENCY
Washington, DC 20305

Destroy this report when it is no longer needed. Do not return to sender.

PLEASE NOTIFY THE DEFENSE NUCLEAR AGENCY, ATTN: STTI, WASHINGTON, D.C. 20305, IF YOUR ADDRESS IS INCORRECT, IF YOU WISH TO BE DELETED FROM THE DISTRIBUTION LIST, OR IF THE ADDRESSEE IS NO LONGER EMPLOYED BY YOUR ORGANIZATION.

UNCLASSIFIED

SECURITY CLASSIFICATION OF THIS PAGE (When Data Entered)

REPORT DOCUMENTATION PAGE		READ INSTRUCTIONS BEFORE COMPLETING FORM
1 REPORT NUMBER DNA-TR-81-158	2 GOVT ACCESSION NO. A131274	3 RECIPIENT'S CATALOG NUMBER
4 TITLE (and Subtitle) NUCLEAR-INDUCED LIGHTNING AURORA EXPERIMENT		5 TYPE OF REPORT & PERIOD COVERED Technical Report 6 PERFORMING ORG. REPORT NUMBER MRC/SD-R-103
7 AUTHOR(s) J.W. Erler W.G. Vulliet B.C. Passenheim V.A.J. van Lint		8 CONTRACT OR GRANT NUMBER(s) DNA 001-81-C-0151
9 PERFORMING ORGANIZATION NAME AND ADDRESS Mission Research Corporation 5434 Ruffin Road San Diego, CA 92123		10 PROGRAM ELEMENT PROJECT TASK AREA & WORK UNIT NUMBERS Task X99QAXVC-00002
11 CONTROLLING OFFICE NAME AND ADDRESS Director Defense Nuclear Agency Washington, D.C. 20305		12 REPORT DATE 11 August 1982 13 NUMBER OF PAGES 68
14 MONITORING AGENCY NAME & ADDRESS (if different from Controlling Office)		15 SECURITY CLASS (of this report) UNCLASSIFIED 15a DECLASSIFICATION DOWNGRADING SCHEDULE N/A

16 DISTRIBUTION STATEMENT (of this Report)

Approved for public release; distribution unlimited.

17 DISTRIBUTION STATEMENT (of the abstract entered in Block 20, if different from Report)

18 SUPPLEMENTARY NOTES

This work was sponsored by the Defense Nuclear Agency under RDT&E RMSS Code B323081466 X99QAXVC00002 H2590D.

19 KEY WORDS (Continue on reverse side if necessary and identify by block number)

EMP
Ivy Mike
Nuclear Lightning
Radiation
Nuclear Explosions
Source Region EMP

20 ABSTRACT (Continue on reverse side if necessary and identify by block number)

Nuclear lightning has been experimentally produced at AURORA. The propagation velocity, the current carried by the streamer and other parameters were measured. The results are compared with existing models.

DD FORM 1 JAN 73 1473 EDITION OF 1 NOV 65 IS OBSOLETE

UNCLASSIFIED

SECURITY CLASSIFICATION OF THIS PAGE (When Data Entered)

TABLE OF CONTENTS

LIST OF ILLUSTRATIONS

SECTION 1
INTRODUCTION

Nuclear-induced lightning (NIL) has been observed on several occasions in atmospheric tests in the 1950s and 1960s. Perhaps the best documented shot was Shot Mike of Operation Ivy on Eniwetok Atol on October 31, 1952 (Ref. 1). Shot Mike was a 10.4 MT detonation which triggered at least 5 lightning flashes which grew from the region of a construction camp on one side and from water on the other ≈1 km from ground zero, to heights in excess of 600 m where their further development was obscured by cloud cover. One frame from a movie is shown in Figure 1. These were first noted at ≈1 ms after zero time and persisted for ≈75 ms. Calculations would suggest that the electric fields in the vicinity of these lightning strikes were about 3×10^4 V/m and that the dose in this vicinity was $\approx 3 \times 10^7$ rads/s (Ref. 2). Propagating strikes were observed with high speed photography and from these records one may infer a propagation velocity of ≈1 to 2 x 10^7 cm/s.

Nuclear-induced lightning appears to differ from natural lightning in some respects. First NIL appears to grow at a nearly constant rate persisting for 10's to 100's of milliseconds, whereas natural lightning's growth is discontinuous, exhibiting peak currents of $\approx 10^4$ A developing in times of $\approx 10^{-7}$ s ($\dot{I} \approx 10^{11}$ A/s) with a fall time for the first stroke of ≈50 μs. Second NIL appears to propagate at a slower velocity and in lower electric fields. Third there is no evidence of a stepped leader which is normally associated with natural lightning. Although nuclear lightning transports lower peak currents than natural lightning it persists so long that it delivers more total energy to the lightning rod. (The continuing current in natural lightning may persist for seconds at <u>very</u> low levels.)

Figure 1. Lightning strokes observed on IVY MIKE event. Numbers are ground ranges in meters; the lightning channels have been inked for better reproduction.

The significance of NIL is that it may represent an electromagnetic threat to systems that would otherwise survive. For example, NIL might couple to antennas or the power distribution systems of blast-hardened shelters.

While NIL has long been known, it was only recently that a model was created to explain its characteristics (Ref. 2,3). In this model, electrostatic fields are produced by photoCompton currents which are driven from the detonation point by ionizing radiation and by the return current through the comparatively conducting earth or sea surface. While these electric fields are not sufficient to produce ordinary electrostatic air breakdown ($\approx 3 \times 10^6$ V/m), they are sufficient to produce large current densities in air which has been rendered conductive by ionizing radiation. If one imagines an initiation point (such as the antenna or structural towers observed in Shot Mike), one may calculate a radius within which the electric fields achieved an avalanche value ($\approx 3 \times 10^6$ V/m). Whereas the electric fields are fixed within this radii, the current density increases as r^{-2}, so that within a smaller region of radius "a" the inwardly flowing power density is sufficient to (adiabatically) heat the enclosed air to a temperature which will support thermal ionization ($\approx$1 eV or 11,200°C). Thermally ionized air produces a small conductive bubble which subsequently runs into a filament of nearly constant radius which burns its way along at a rate determined by the rate air is thermally ionized at the tip of the discharge (Ref. 2,3). This model is schematically represented by Figure 2.

When the present investigation was undertaken, there were still significant uncertainties concerning the validity of this model. We judged that if the model were valid and could be extended to laboratory simulator conditions (i.e., AURORA) by using the scaling relations given by the model, that the credibility of the model would be substantially enhanced. Consequently a laboratory experiment was devised (Ref. 4). Inasmuch as no laboratory simulator can provide the dose rate associated with an atmospheric test, over the dimensions and duration of an atmospheric test, considerable

PROPAGATION VELOCITY

For $r > R$ (Ohmic)

$J = \sigma E = K\dot{D}E \quad E < E_a$

For $r > R$ (Avalanche)

$E \equiv E_a \quad J = \sigma E_a (R/r)^2$

$P = JE_a$

Inside $r \sim a$ (Thermal ionization)

$$v = \frac{Pa}{Q} \sim \frac{K\dot{D}(E_a R)^2}{Qa}$$

Experimentally $E_a R \approx V_{appl}$

$\dot{D}$ measured

a estimated

$Qax \approx \int \sigma V^2 dt, \quad \sigma = K\dot{D}$

$Qax \approx \int IV dt$

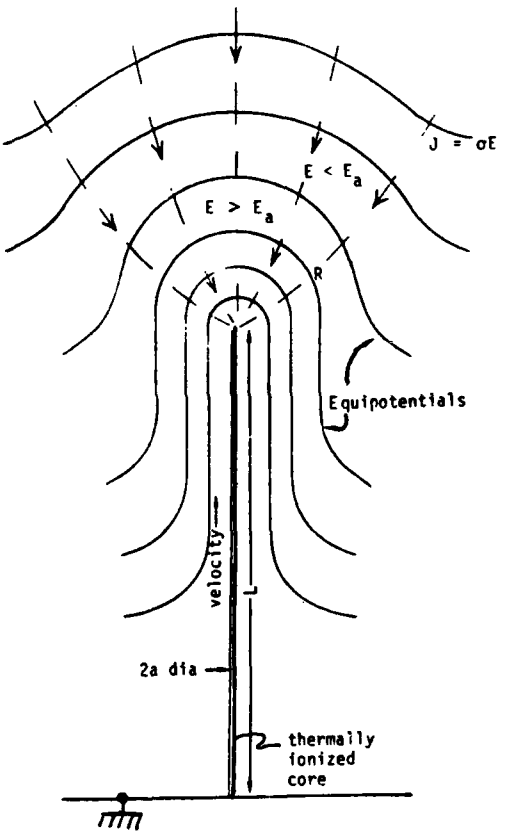

Figure 2. NIL model.

scaling was required. Reference 4 suggested that applying ≈ 100,000 volts across a spark gap in air exposed to $\approx 10^{11}$ rads/s would result in an avalanche region with a radius of approximately 1.6 cm. The predicted propagation velocity depends on the instantaneous power density, assuming a propagation velocity of $\approx 10^7$ cm/s (from Reference 1) and an AURORA pulse width of ≈120 ns, the NIL is expected to be no more than ≈1 cm long.

The AURORA experiment was designed to duplicate the conditions thought to exist at the tip of a propagating nuclear lightning. The AURORA simulator provided a radiation pulse to create the conductive air. The PULSAR model 5Q (100 kV) pulser was syncronized to the AURORA pulse to provide the electric field. In a three day test period, the experiment was set up, executed and torn down. At least five events were observed that exhibited the charactersitic of a NIL. Specifically, that they originated at a point of high field concentration, propagated at a velocity of $\approx 2 \times 10^7$ cm/s, and persisted only while the radiation pulse provided conductive air.

Nuclear induced lightning can only occur during the radiation pulse. Any streamer that draws current before or after the radiation pulse is not NIL.

A description of the experiment is presented in Section 2, Experimental Design. The results are presented in Section 3. They are divided into two parts: diagnostics and nuclear lightning results.

SECTION 2
EXPERIMENT DESIGN

The objective of this experiment is to characterize the behavior of a lightning stroke in dosed (conductive) air. In this experiment we created conditions indentical to those postulated to exist at the tip of a NIL streamer over (limited) dimensions determined by the capabilities of the radiation source (dose rate and pulse width) and electrical pulser (voltage and stored energy). The electrical pulser was carefully synchronized to the AURORA photon pulse. The electrical conditions were measured with voltage probes and current sensors. Radiation conditions were determined from TLD dosimetry (dose) and transient "pulse shape" by dose rate sensors. The NIL event was sensed electrically and optically. An optical system (dubbed a macro-scope) was used to measure the discharge propagation characteristics. This system had 5 fast detectors each of which viewed a 2.5 mm wide strip of the object. Open shutter photographs were obtained. In this experiment we created a radiation induced electrical streamer. The key characteristics to be investigated include:

a) The propagation velocity of the NIL;
b) The current carried by the NIL;
c) The applied field
d) The boundary layer potential developed at the cathode;
e) The dependence of a), b), and c) on the dose rate;

2.1 TEST CHAMBER DESIGN

The test chamber geometry was designed to produce fields sufficient to produce an avalance region large enough for a streamer of measurable length to occur. A Pulsar Pulsepak 50Q (100 kV, 200 J) pulser was used to create the required fields. The 50Q was triggered by the Pulsar 10A (10 kV) trigger generator. The geometry is limited to one where 100 kV is sufficient to create the avalanche field and 200 J is sufficient to provide current during the 120 ns AURORA pulse. The geometry in Figure 3 meets these requirements. The hemispherical cathode tends to concentrate the current flowing to the pin and reduce the current flowing to the ground plane. The electric field at the tip of the pin could be slightly adjusted by changing the distance between the hemisphere and the ground plane. The radius of the tip of the pin is 1.2×10^{-2} cm (0.005"). The test chamber was a plexiglass box. The chamber was mounted on a wooden frame to place it at the height of the AURORA radiation "hot spot". A photograph of the chamber mounted on the structure at AURORA is shown in Figure 4.

2.2 ELECTRICAL MEASUREMENTS

In order to electrically characterize this laboratory simulation of NIL we equipped the experimental test chamber with a number of voltage probes and current sensors. This measuring apparatus is schematically indicated in Figure 5. Voltage from a 100 kV Pulsar model 50Q pulser was applied between a 0.025 cm (0.010") diameter wire anode and a hemispherical 25 cm diameter stainless steel cathode. The voltage applied to the cathode (which was negative with respect to ground) was measured with two voltage probes. The first voltage probe was comprised of a 28 kΩ resistor string, made from twenty 1.4 kΩ resistors and a 1.8 Ω measurement resistor. The response time of this probe is ≈28 ns (Ref. 5). A second voltage probe with greater sensitivity and faster response time (≈10 ns) was comprised of a 5.4 kΩ resistor string composed of forty 135 Ω resistors and a 1.8 Ω

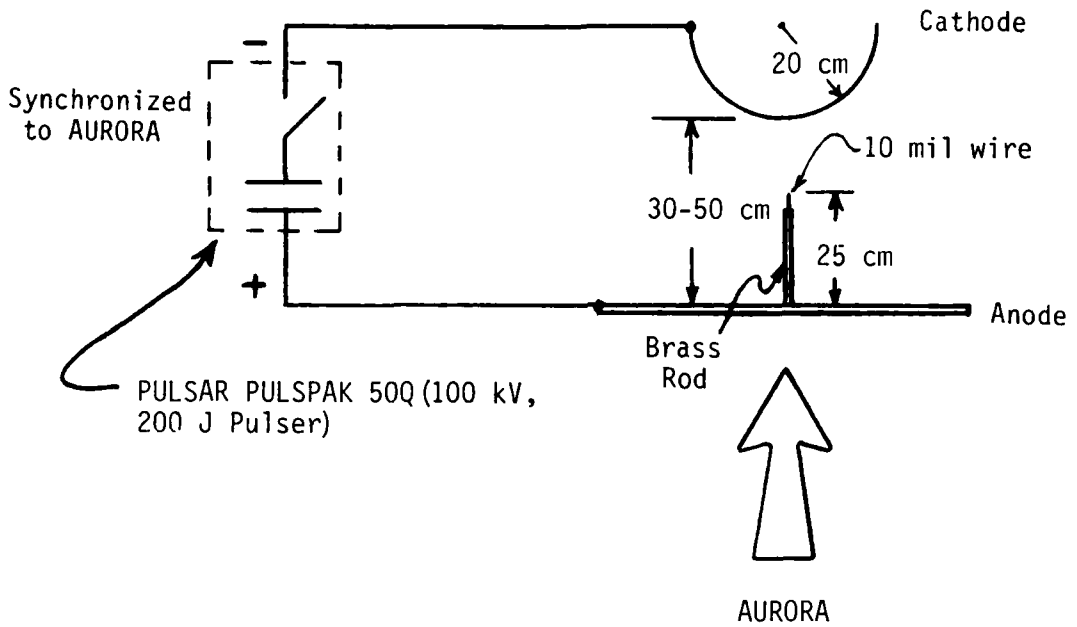

Figure 3. Test chamber geometry.

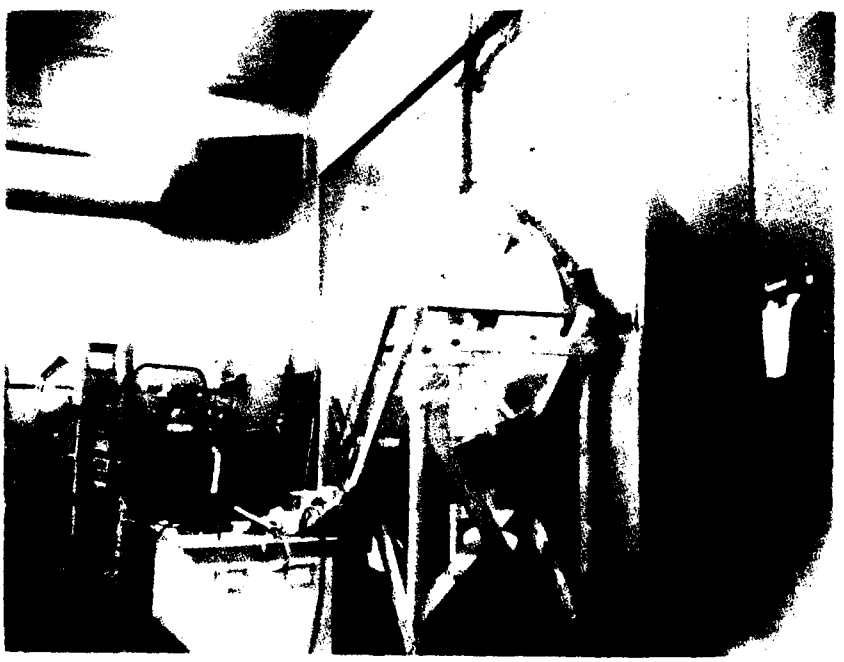

Figure 4. Test chamber at AURORA.

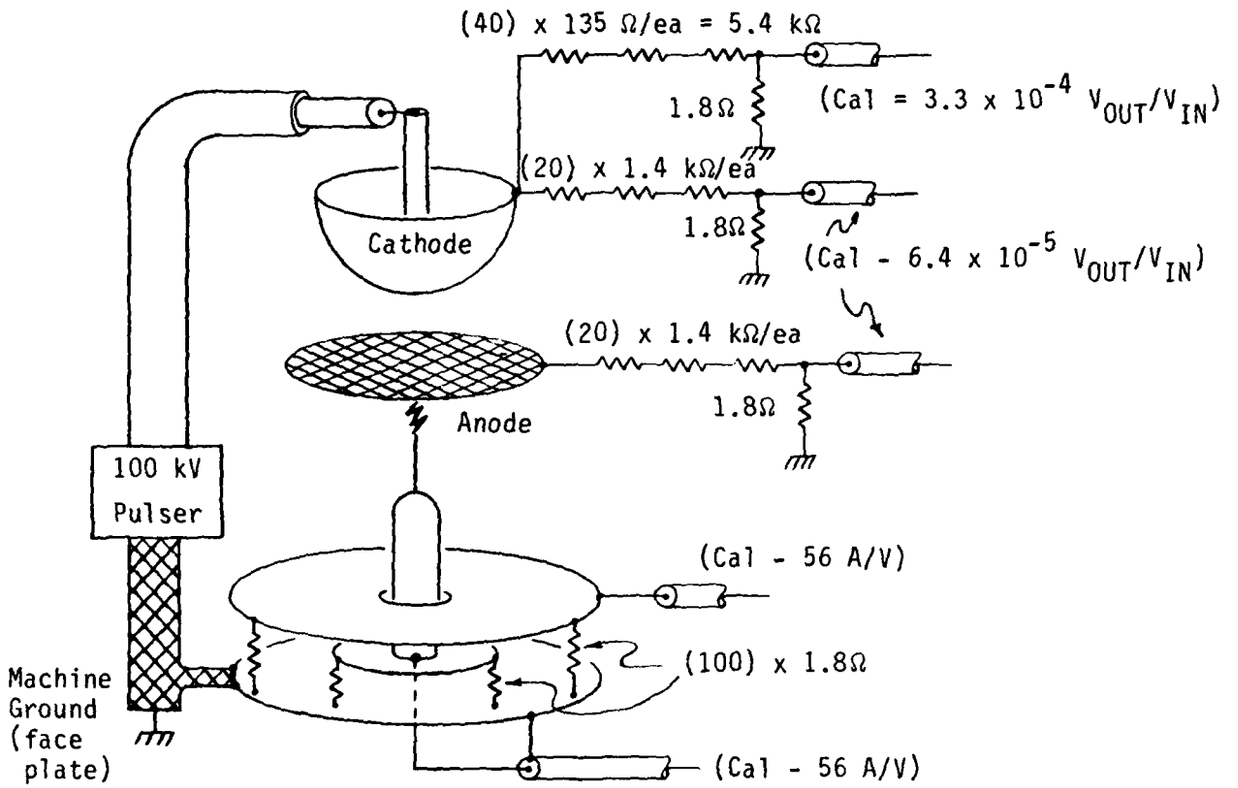

Figure 5. Schematic representation of electrical voltage probes and current sensors.

measurement resistor. Because a non-uniform voltage drop can occur at the cathode (sometimes called cathode fall) a grid Langmuir probe was installed ≈2 cm away from the cathode. The Langmuir probe voltage was monitored with another 28 kΩ, 1.8 Ω voltage divider. The Langmuir probe is described in Appendix 1.

Radiation induced photo-currents in the probe and resistor string were considered to determine the probable signal to noise. Photocurrents generated were expected to be intermediate between the Compton current from the probe area ($\approx 10^{-10}$ Coul/rad-cm^2) and the replacement current in the coaxial cable ($\approx 10^{-13}$ A-s/rad-m). The overall length of the voltage probe and the associated cabling was ≈ 1 m. The peak dose rate at the probe was $\approx 10^{11}$ rad/s. Thus, the radiation-induced currents are intermediate between 10 mA and 1 A. The anticipated signal was generated by ≈ 3 A across the sensing resistor, which was larger than the expected radiation-induced currents.

To measure currents to the pin anode or annular ground plane we measured voltages across low resistance resistors, as shown in Figure 6. To be sure this measurement is correct one must assure oneself that the shunt resistance of radiation dosed air is large by comparison. The resistance between the large annular plate and the ground plate due to the conducting air can be calculated from,

$$R = \frac{d}{A\sigma}$$

where d is the plate separation, A is the plate area and σ is the conductivity of the dosed air. σ is calculated from,

$$\sigma = K \dot{\gamma} e \mu/a$$

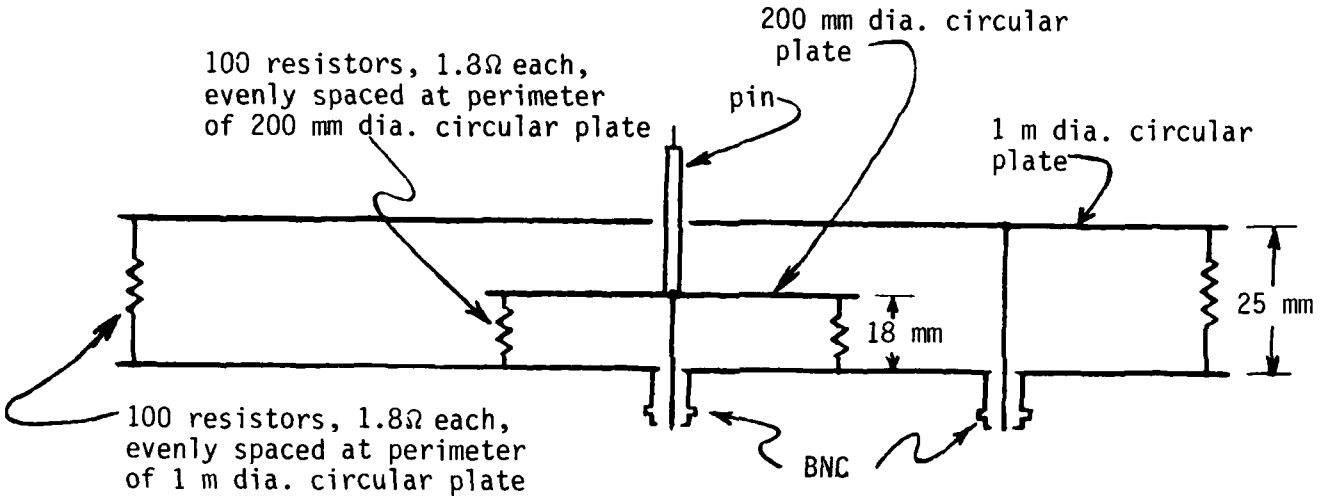

Figure 6. Cross section of low impedance voltage divider current sensor.

where K is 2.2 x 10^9 $cm^{-3}rad^{-1}$, μ/a is 2 x 10^{-5} cm^2/V for damp air, e is the electron charge (1.6 x 10^{-19} Coul) and γ is the gamma dose rate (rad/s). For a gamma dose rate of anything less than 1 x 10^{11} rads/s (maximum observed dose) and two 1 m diameter plates separated by 2 cm , the resistance between the plates is about 0.4 Ω. The measuring resistor between the plates was set at 0.018 Ω so that more than 95% of the current flowed through the resistors. The responsivity of the sensor is 55.6 A/V. Since currents ≈30 A were expected, 500 mV signals should be observed.

The resistance between the smaller pin plate and the ground plate due to the conducting air was ≈100 Ω. The pin was expected to draw ≈100 to 1,000 A. To generate signals between 1 and 10 volts, the resistance between the pin plate and the ground plate was 0.018 Ω. The resistance between the plates in both cases was accomplished by connecting 100 1.8 Ω resistors in parallel. The voltage across the plates was fed via RG-58 cables to the data room and recorded on oscilloscopes.

2.3 OPTICAL MEASUREMENTS

The propagation velocity of the NIL was measured optically. The optical system can be divided into two categories: a) light collection and delivery to the data room; b) image processing and recording.

The light was collected with two parabolic mirrors placed at positions around the NIL 90° apart as shown in Figure 7. The mirrors were mounted on mirror mounts to allow for angular adjustments. The mirror mounts were mounted on translation stages to allow for movement along the optical axis to focus the mirrors. The tip of the pin in test chamber was located 1.8 m above the floor (the height of the AURORA "hot spot"), with the test chamber placed as close to AURORA as possible. The two beams were sent via routing mrirors (mounted on mirror mounts and tripods) through the optical port into the data room. The beam routing system is represented in

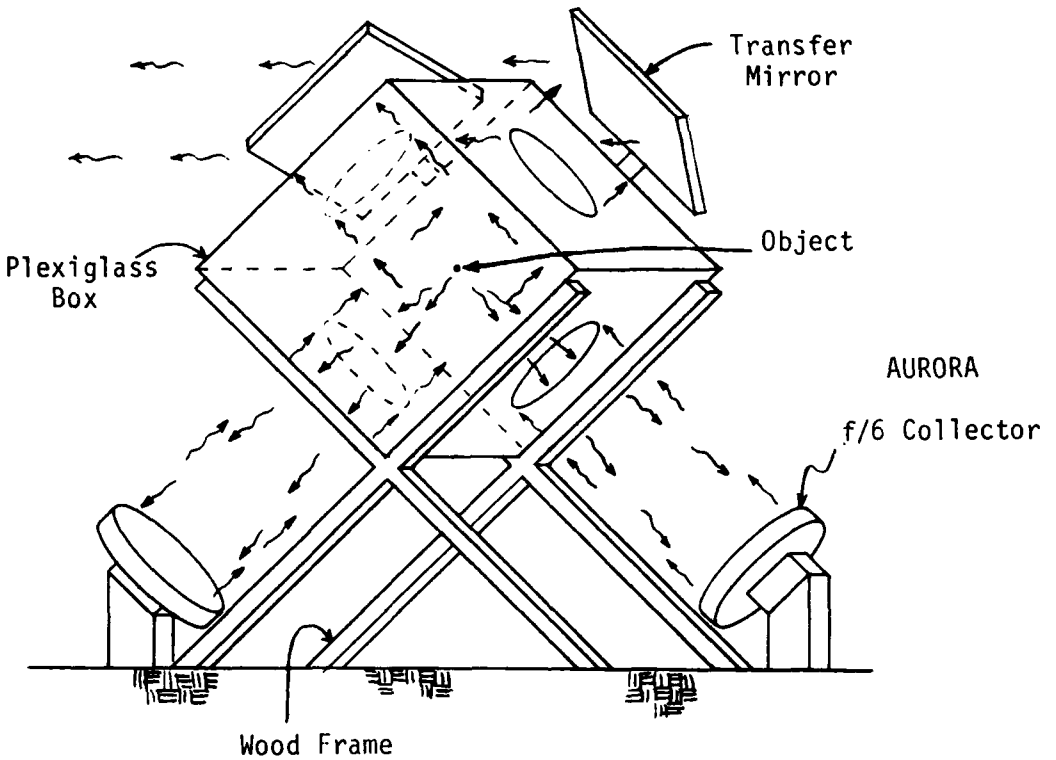

Figure 7. Test chamber and parabolic collection/collimation mirrors. Light from the lightning falls on a pair of 30 cm diameter parabolic mirrors which collimate the light and send it back through the test chamber to 45° flat transfer mirrors which deflect it away from AURORA toward the imaging optics.

Figure 8. The optical port was located ≈1.8 m off the floor. The beams were reflected from the optical port to the image processing and recording system in the data room. Seven mirrors were required to collect and transfer the image of the NIL to the data acquisition room. The seven mirror surfaces are thought to have a reflectivity of ≈ 80% each, resulting with an overall transmission of 21%.

The image of the NIL was recorded both photographically and electro-optically. The optical components of the imaging system are shown in Figure 9. Five avalanche photodiodes (APDs) were placed in a horizontal line 1 cm apart. A 1 cm diameter lens with a focal length of 0.8 cm was placed in front of each photodiode. The output of each APD was fed into an amplifier with a gain of 13 to 15 dB and an input impedance of 50 Ω. These were the receivers of the DNA/HDL high speed fiber optic links. The output of the amplifiers was fed via RG58 cables to the oscilloscopes. The rise time of the APD-amplfier combination was ≈1 ns. The published spectral response of the APDs is shown in Figure 10.

In Figure 11 the optical components of one beam are shown. To evaluate the magnification and the power losses in the system, the system was evaluated in the direction of light travel (from left to right). Light from the (1 cm long) source entered reflector A (represented in Figure 11 by a lens) set a distance f_A (192 cm) from the source. The energy from the source radiates isotropically. The optical efficiency of this reflector is the ratio of light captured by a mirror of radius, r, ($A_1 = \pi r^2$) to the area of a sphere whose radius is the mirrors focal length ($A_2 = 4\pi(f_A)^2$, ($r \approx$ 15 cm, $f_A \approx$ 192 cm). This is 0.15%. Lens C, placed 30 m to the right of reflector A, will create an image 100 cm to its right. The beam between optics A and C is collimated. The image (L) is located at the focus of lens C by the thin (lens formula),

$$\frac{1}{I} + \frac{1}{O} = \frac{1}{f}$$

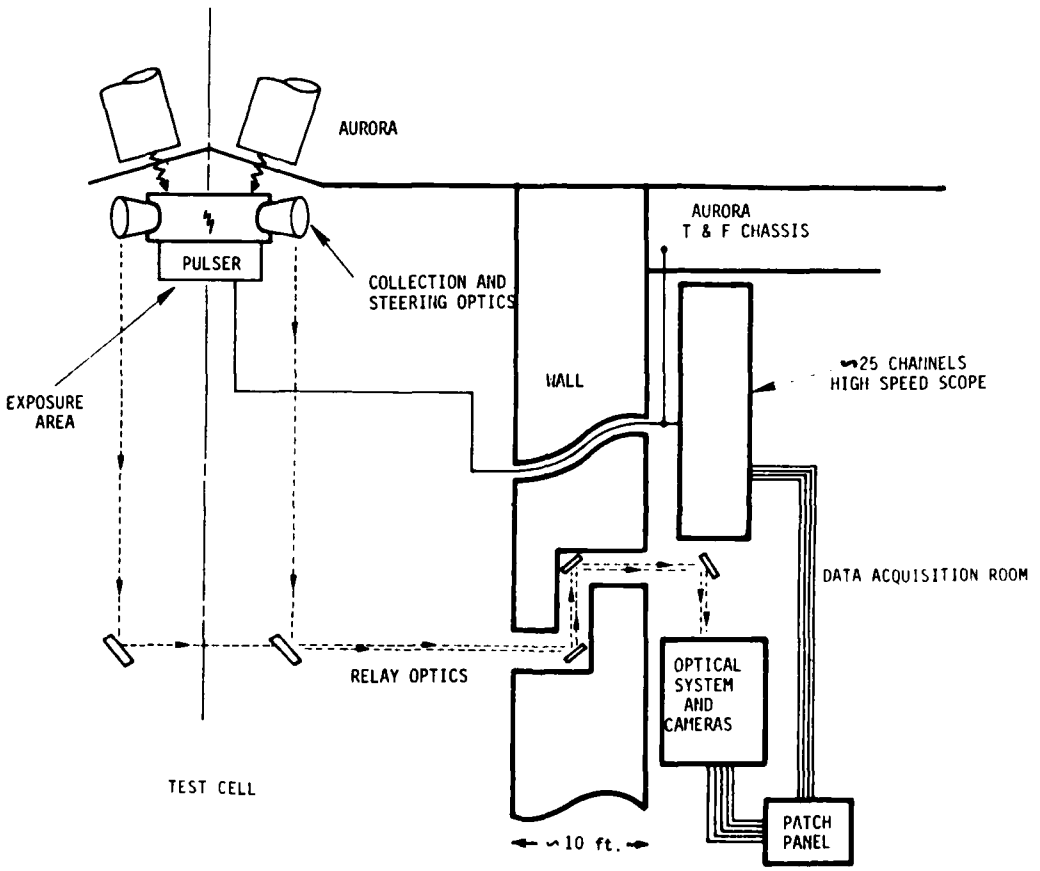

Figure 8. Overhead view of the optics system (macroscope) designed to form unity gain image of the nuclear lightning in the data acquisition room about 70 feet away.

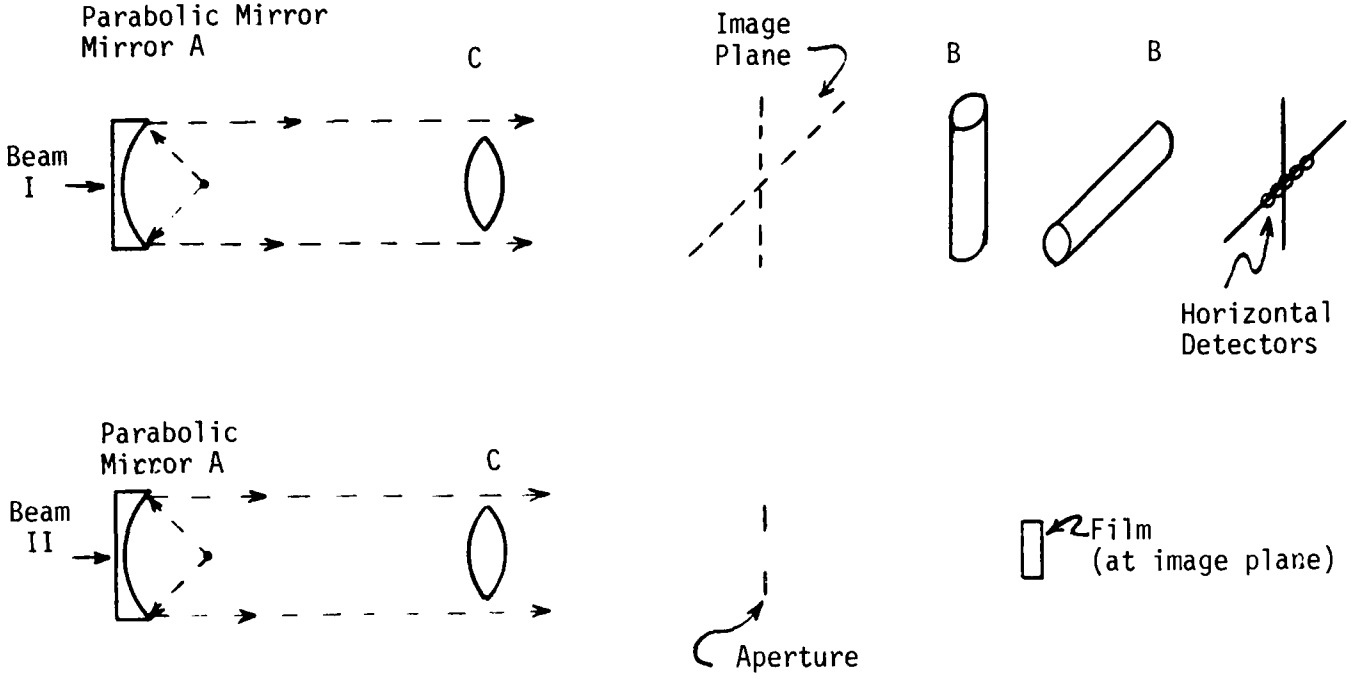

KEY:

Component	Diamater	Focal Length
Reflector A	31 cm	191 cm
Lens C	4.7 cm	100 cm
Cylindrical Lens B	5.7 cm x 40 cm	8.6 cm

Figure 9. Optical system components.

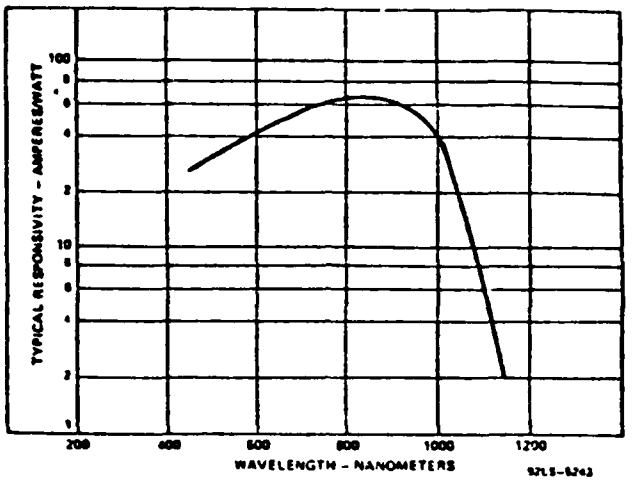

Figure 10. Typical spectral responsivity of APDs.

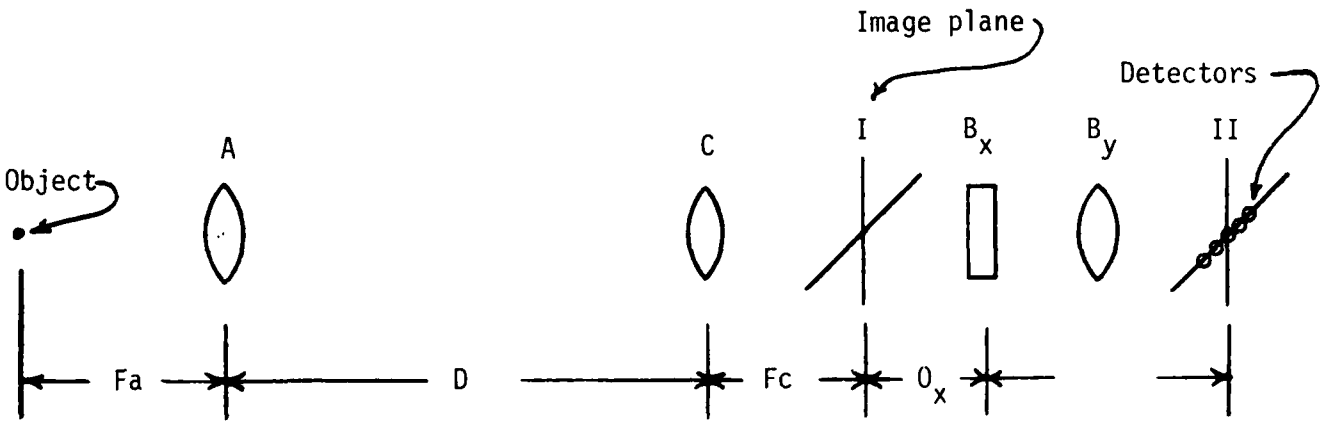

KEY:

Component	Diameter	Focal Length
Reflector A	31 cm	191 cm
Lens C	4.7 cm	100 cm
Cylindrical Lens B_x & B_y	5.7 cm x 40 cm	8.6 cm

Figure 11. Optical component placement of Beam I.

where the object distance (0) is finite (∞) for collimated light. The magnification at this image is given by

$$M = \frac{f_c}{f_A} = 0.52$$

where f_c and f_A are the focal lengths of lens c and mirror A. The magnification was set to unity by adjusting the distance from the object to collector A and the distance from the lens to the focal plane. The size of image at the image plane is then ≈1 cm. The beam is 22 cm in diameter as it passes through lens C, which is 4.4 cm in diameter. From the ratio of the areas of the beam and the lens, only 10% of the energy caught by the parabolic reflector goes through lens C.

The reader should notice that all the optics used in this investigation were "off the shelf". This resulted in a less than optimally efficient system. Should more efficiency be required in further investigations we are confident that at least a decade more collection efficiency is feasible.

After passing through image plane I, the beam enters cylindrical lenses B_x and B_y. The magnification performed by these lenses is 4.0 in the "X" dimension and 0.25 in the "Y" dimension. The purpose of the cylindrical lenses is to give each detector a band shaped field-of-view, narrow in the arc propagation direction and wide perpendicular to the propagation direction. Since the two cylindrical lenses are orthogonal, the image-object relationship can be treated independently for each lens. Assuming a source which is 1 cm in <u>both</u> dimensions, the image in plane II will be 4 cm in the X dimension and 0.25 cm in the Y dimension. Of course, the NIL was essentially a line - so this represents the <u>maximum</u> excursion of the image in each direction. All of the light passing thorugh lens C will also find its way through B_x and B_y.

The diameter of the detectors in image plane II is 0.8 mm. As mentioned earlier, 8 mm focal length, 1 cm diameter lenses were placed in front of each detector. In the "Y" dimension, the beam is 4 cm wide. With 5 detectors, the exposed "area" is 4 cm (4 detectors). Therefore, in the "X" dimension, ≈ 25% of the energy falls on a detector. About 4% of the power is lost by reflection at each surface of lenses C, B_X, B_Y and the 1 cm lenses at the photodiodes, resulting with a loss of 28%. The spectral transmission of the lenses is shown in Figure 12. The transmission of each lens is ≈ 90%, resulting with a transmission of 66% for all 4 lenses. We estimate the total system efficiency is:

percent of NIL power sent to each detector =

(0.15%) reflector capture ratio	×	(21%) mirror losses	×	(72%) lens reflective losses	×	(66%) lens transmission	×	
(4.4%) lens C	×	(25%) along the NIL's direction	×	(100%) perpendicular to the NIL			=	1.65×10^{-4}%

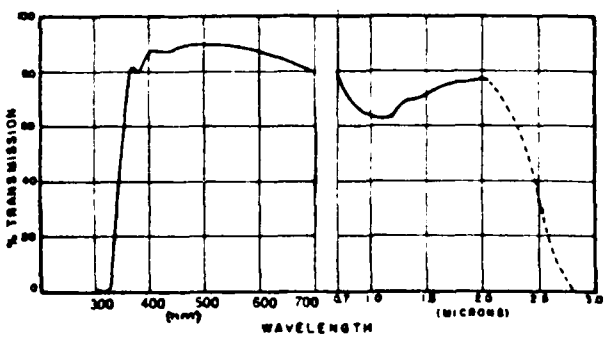

Figure 12. Lens Spectral Transmission Curve.

The optical systems sensitivity is estimated here to be 1.65 μW/W. The responsivity of the APDs shown in Figure 10 indicates an average responsivity in the visible range of 40 A/W. Combined with the amplifier gain the APD response is 9.3 kV/watt (watt on the detector). The overall optical system response (from source power to APD-amplifier output voltage) is thus estimated to be ≈15 mV/W.

Polaroid film was a placed at image plane I of beam II. The spectral sensitivity (cm^2/erg) required of the film can be calculated from:

$$S = \frac{D}{P\tau}$$

where D is the area of the image on the film (cm^2), τ is the pulse length (seconds) and P is the radiated power at the film (erg/s). For a 1 cm x 0.02 cm image, D is 2 x 10^{-2} cm^2. The AURORA pulse is 120 ns FWHM, so τ is ≈120 ns. For 10 Watts (10^8 erg/s) from the object in this spectral region the power at the film (P) is 10^8 erg/sec x 6.4 x 10^{-6} (system transmission) ≈640 ergs/s. The required spectral sensitivity is then 260 cm^2/erg. The spectral sensitivity of Polaroid Type 612, ASA 20,000, is ≈1,000 cm^2/erg. This is substantially more sensitive than Type 47, ASA 3,000 film which has a spectral sensitivity of ≈100 cm^2/erg. Type 612 film was used. This calculation suggests Type 612 was more than sufficiently sensitive, whereas Type 47 would have been marginally adequate.

Variable apertures were placed in the system to limit the intensity of the beam, if required. All lenses, apertures and detectors were mounted on X-Y translation stages to facilitate centering and adjusting the beam. All of the optics were mounted on aluminum rails. The rails were mounted on 1" thick plywood which was placed on a sturdy table. The polaroid film was held in an oscilloscope camera back. The metal slide was used

as a manual shutter. Optical alignment was performed by placing a 600 watt tungsten iodide bulb at the arc location and adjusting each element, starting with those nearest to the bulb.

2.4 OPTICAL SYSTEM CALIBRATION

The optical system was calibrated by using the 600 watt tungsten light bulb with a 1 cm long filament as a source. The light from the light bulb passed through the optical system in precisely the same manner as the light from the NIL (with the exception of a 50% transmission neutral density filter in the optical path). Since the APD's amplifier is AC coupled, the calibration of the system using a continuous light source must be performed without using the amplifiers. To do this, the current through the 50 Ω input impedance of the amplifiers was measured. The 1 cm long filament source was projected onto the lenses in front of four photodiodes. Each photodiode received 25% of the light from the filament. The tungsten filament operated at about 3400 K. It has been estimated that 10% of the lamp power is radiated in the visible spectral region (Ref. 6). From this estimate the 600 W bulb used for this calibration will radiate 60 W of visible light (the remainder is mostly IR). The sensitivity of the system can be calculated from the current amplifier gain, bulb power and neutral density filter losses:

$$\frac{\text{(Photodiode current)x(Amplifier input impedance)x(Amplifier voltage gain)}}{\text{(0.50 N.D. Filter transmission) x (60 watts) x (0.25)}} = \text{sensitivity (V/watt)}$$

The results of this measurement are shown in Table 1. The average sensitivity of the photodiodes is 14.8 ± 3 mV/watt. The uncertainty principally reflects uncertainties in the APD and amplifier gains. In this test we did not independently check the output of the light bulb or the accuracy of the

neutral density filter. The National Bureau of Standards provides suitable services for a price. The spectrum of the arc was predicted (Ref. 7) to be different than that of a gray body radiation (i.e., the light bulb). The spectra of the filament reference source, and the NIL, and the spectral response of the optical system must be considered when calculating the total radiated power from the NIL. Care must also be taken to assure that the lenses in front of the photodiodes are completely filled. This is assured if signals are observed on the two adjacent photodiodes.

Table 1. Optical system calibration data.
(600 W, 3400°K tungsten filament source)

APD	Current	Sensitivity
1	50 μA	10.4 ± 2 mV/w
2	80 μA	16.6 ± 3 mV/w
3	95 μA	19.7 ± 3 mV/w
4	60 μA	12.4 ± 2 mV/w

2.5 FACILITIES, TIMING SEQUENCE AND DATA ACQUISITION

The Pulsar 50Q pulser was placed within a few (< 10) feet from the test chamber to eliminate the difficulties in matching the load of the chamber to a long coaxial cable.

The throughput delay from command to firing of the pulser is 250-350 ns, with ± 2 ns jitter. The delay of AURORA from the Marx erection trigger is 1.3 μs. We were told this delay had a ± 50 μsec jitter but (for constant charging parameters) we observed far less. The width of the AURORA pulse is ≈ 120 ns at FWHM. To insure that the pulser is on during AURORA, the pulser was fired "just" prior to the AURORA pulse (i.e., ≈5 ns).

The pulser was fired using the timing circuit in Figure 13. The position of the pulser firing relative to the AURORA radiation pulse can be

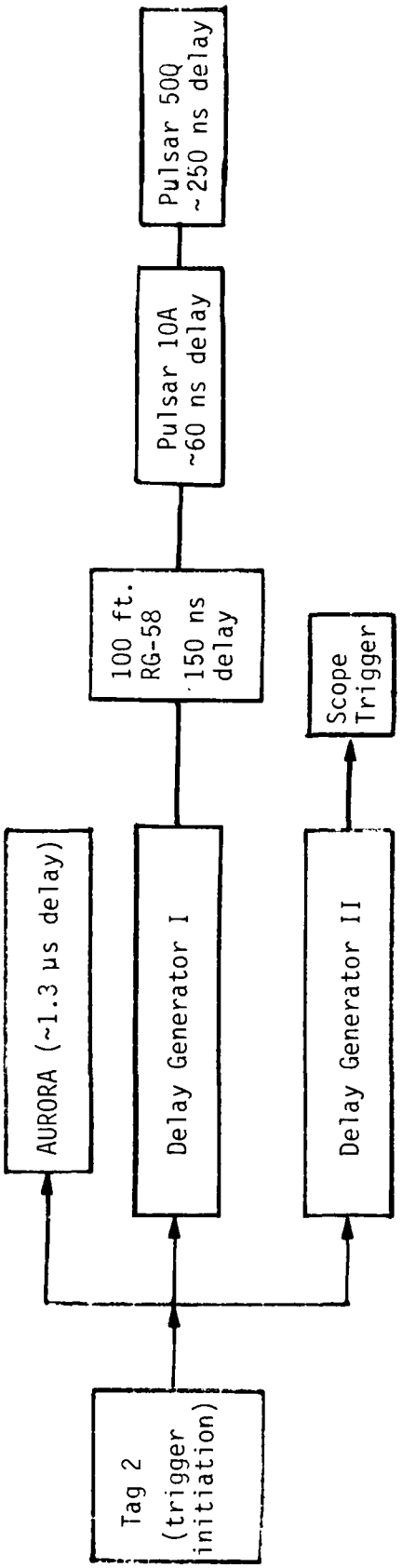

Figure 13. Trigger circuit.

adjusted using delay generator I. Delay generator II is used to simultaneously trigger all the oscilloscopes prior to both the pulser and AURORA firing.

The data was acquired with ≈25 oscilloscope channels and photographs of the NIL. Some signals were redundantly recorded at different gains and/or sweep speeds.

The pulser and instrumentation grounding was performed using the circuit in Figure 14. The cable carrying the trigger signal to the 10 A was placed outside the overall shield and connected to the trigger output in the data room through a pulse transformer. This was done because a high voltage spike was discovered on that cable when the 50 Ω, 100 kV pulser fired (i.e., the Pulsar 50Q sent a noise pulse back down its own trigger line to the instrumentation room ≈300 ns after it received a trigger from the Pulsar 10A). When the cable was in the shield it injected noise on the signal cables.

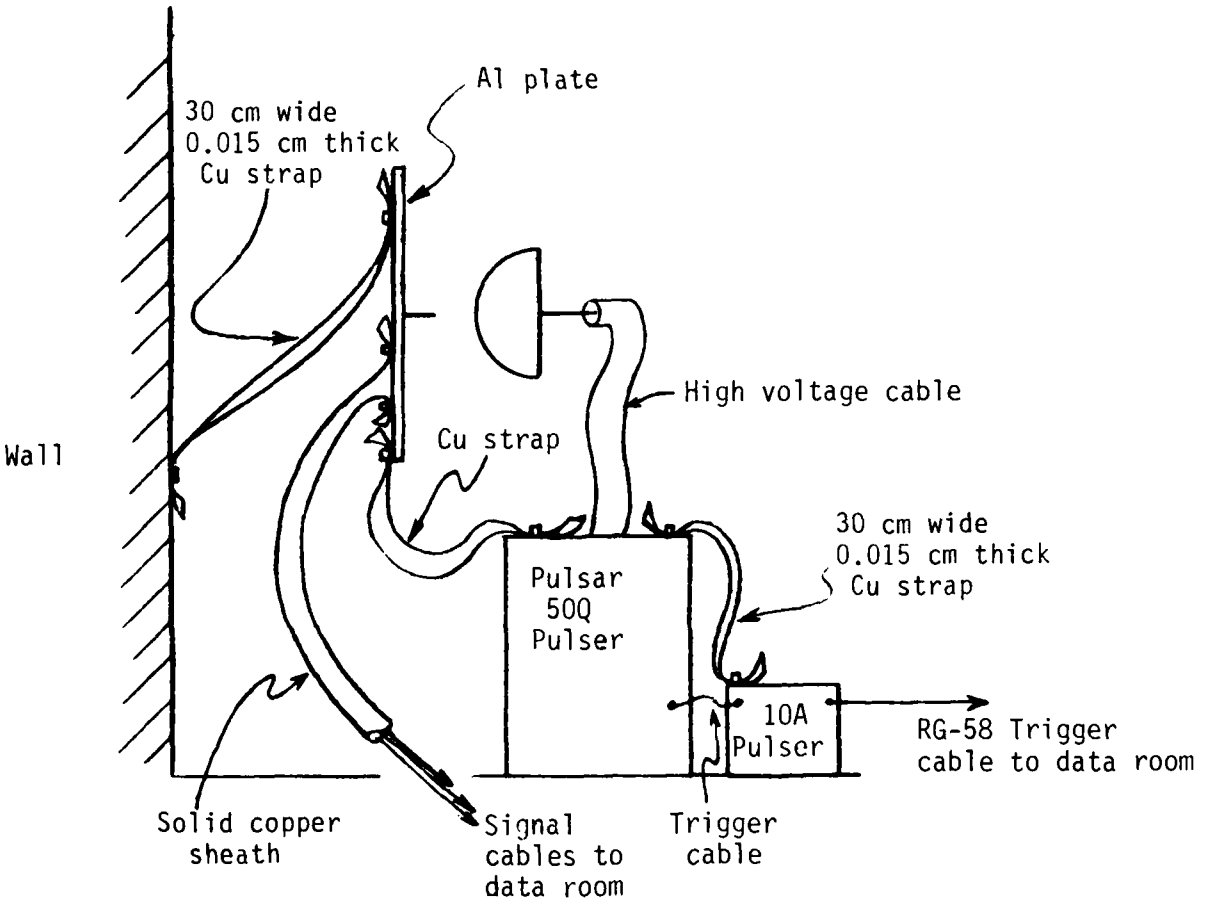

Figure 14. Grounding and shielding system.

SECTION 3
EXPERIMENTAL RESULTS

The experimental results will be presented in two sections: diagnostics and nuclear lightning results.

3.1 DIAGNOSTICS

3.1.1 100 kV Pulser Behavior

Scope photos of the voltage on the pulser with and without the AURORA radiation pulse are shown in Figures 15A and 15B. The pulser oscillates because it is not terminated in its characteristic impedance (50 Ω). It is initially terminated in essentially an open circuit. In Figure 15B the voltage is clamped at around 35 kV during the AURORA radiation pulse. It appears that a large current is flowing somewhere in the circuit. The pulser has an internal inductance of 1 μH. The internal reactance and the external resistance to ground act as a voltage divider. Exactly where the current is flowing to ground is unknown. The currents that are observed on the current ground plates are not sufficient to cause such a voltage drop. Conceivably the current flowed somewhere within the pulser. It is clearly not an arc within the pulser, because an arc would continue to discharge the pulser after the AURORA pulse ceased. Our best explanation is to assume that the current flowed through dosed conductive air. The troube with this explanation is that the pulser, to the best of our knowledge, was completely filled with SF_6 which shouldn't be conductive under these conditions. Only if it were not completely filled, could this be an explanation for the observation. As indicated in Section 2 we expected the pulser to generate

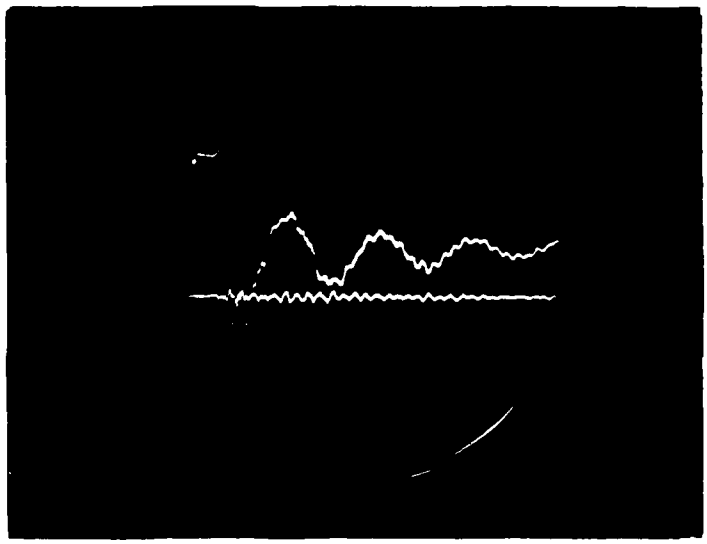

Upper trace:
pulser voltage 31 kV/div

Lower trace:
cable photocurrent
(without AURORA)

horizontal 100 ns/div

Figure 15A. 100 kV pulser without AURORA.

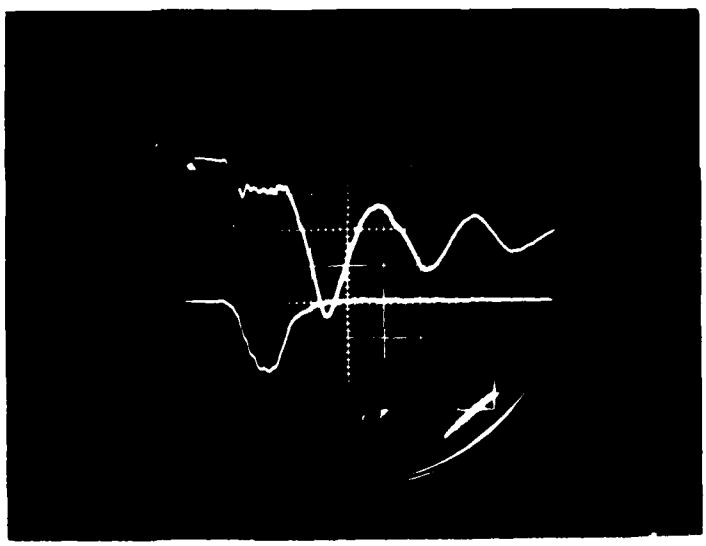

Upper trace:
pulser voltage 31 kV/div

Lower trace:
cable photocurrent
(with AURORA)

horizontal 100 ns/div

Figure 15B. 100 kV pulser with AURORA

100 kV. To compensate for the lower voltage, we adjusted the delay of the pulser so that its natural oscillations would place it on a voltage peak during the radiation pulse. This generated the largest possible voltges. The final timing was such that the pulser fired ≈5 ns prior to the radiation pulse. Notice that such precise timing is only possible if AURORA's operating parameters are the same for every shot.

3.1.2 Current Probe Response

During the tests of the current plates, we discovered that they were inductively coupled to one another. If current is driven onto the inner plate, voltages will show up on both the inner plate (pin) and the outer plate (annular). Those voltages are approximately equal. If a current is driven onto the outer plate, the voltage on the inner plate will be 1/100 of that observed on the outer plate. This means that to determine the current on the outer plate the current on the pin or inner plate must be subtracted from that observed on th outer plate. The current measured on the inner plate (pin) is virtually unaffected by currents on the outer plate. The response of the current plates during a shot in which nuclear lightning was observed is shown in Figure 16A and 16B. An oscillation with a frequency of ≈40 MHz is observed on these signals. We attribute this to LRC oscillations of the current plates.

3.1.3 Grid Response

In Figure 17 the response of the grid and a voltage probe on the pulser output are shown. The voltage indicated on the grid is much smaller than expected. The voltage observed on the grid is apparently due to capacitive coupling to the cathode. It is not known, at this time, why the grid was not charged up by the large current (≈1 kA) passing through it.

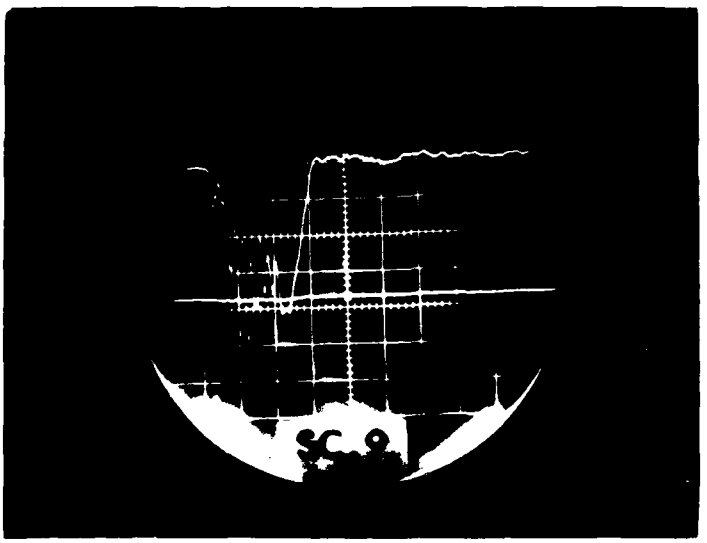

Upper trace:
pin current 111 A/div

Lower trace: extra

100 ns/div

Figure 16A. Pin current with AURORA and 100 kV pulser.

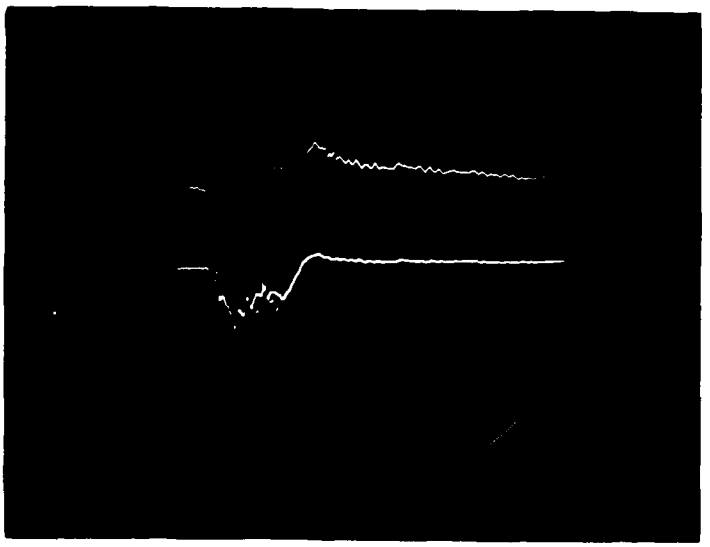

Upper trace:
278 A/div

Lower trace:
1.1 kA/div

100 ns/div

Figure 16B. Large ground plate current.

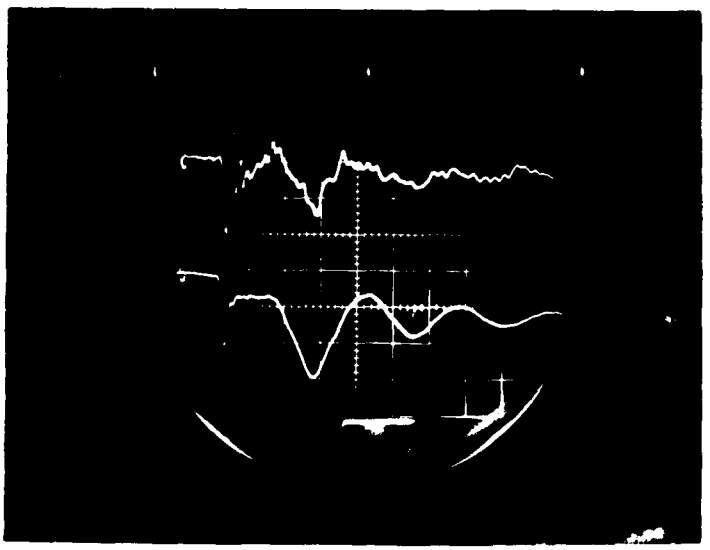

Upper trace:
grid 7.8 kV/div

Lower trace:
applied voltage
60 kV/div

100 ns/div

Figure 17. Grid Response

3.1.4 AURORA Diagnostics

The behavior of the AURORA radiation pulse was monitored using TLD's and gamma-dot sensors provided by the AURORA facility. TLD's were placed in 10 to 15 locations on the test fixture as shown in Figure 18. The total dose and peak dose rate determined from the TLD data for several shots are shown in Table 2. The dose rate of a typical AURORA shot is shown in Figure 19. The TLD's placed inside the cathode are closest to the location of the arc. They indicate a peak dose rate of 9-10 x 10^{10} rads/s.

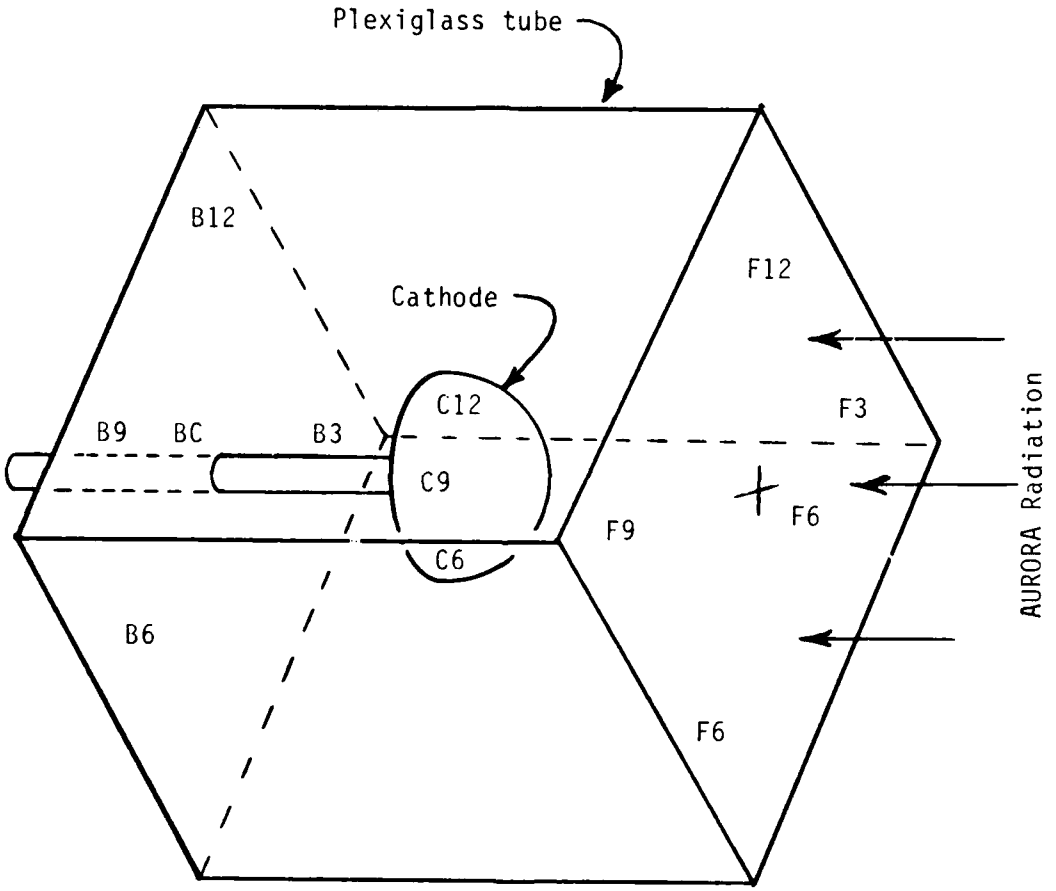

Figure 18. TLD placement.

Table 2. TLD data.

Shot	Position	Peak Dose (per shot) [rads(Si)]	Dose rate [rads/s(Si)]
3702	F3	1.35×10^4	1.06×10^{11}
	F6	1.76×10^4	1.38×10^{11}
	F9	1.43×10^4	1.12×10^{11}
	F12	1.51×10^4	1.19×10^{11}
	FC	1.67×10^4	1.31×10^{11}
	B3	2.72×10^3	2.13×10^{10}
	B6	3.21×10^3	2.52×10^{10}
	R9	3.38×10^3	2.65×10^{10}
	B12	2.76×10^3	2.16×10^{10}
	BC	3.28×10^3	2.57×10^{10}
3708 & 3709	F6	1.11×10^4	8.74×10^{10}
	F9	1.38×10^4	1.09×10^{11}
	F12	1.21×10^4	9.53×10^{10}
	FC	1.46×10^4	1.15×10^{11}
	C6	1.22×10^4	9.61×10^{10}
	C9	1.27×10^4	1.00×10^{11}
	C12	1.18×10^4	9.29×10^{10}
	B9	2.69×10^3	2.13×10^{10}
	B12	2.57×10^3	2.02×10^{10}
	BC	2.82×10^3	2.22×10^{10}
3710 & 3711	F3	9.75×10^3	7.68×10^{10}
	F6	1.17×10^4	9.21×10^{10}
	F9	1.06×10^4	8.35×10^{10}
	F12	1.08×10^4	8.50×10^{10}
	C6	1.37×10^4	1.08×10^{11}
	C9	1.28×10^4	1.01×10^{11}
	C12	1.13×10^4	8.90×10^{10}
	B6	3.16×10^3	2.49×10^{10}
	B12	2.69×10^3	2.12×10^{10}
	BC	2.98×10^3	2.35×10^{10}

Figure 19. AURORA Pulse Shape

3.1.5 Noise Background Shots

Several background shots were performed to determine noise levels on the signals. These include shots where AURORA was fired without the pulser and shots where the pulser fired without AURORA. In Figure 20 the response of a photodiode to the AURORA radiation pulse is shown. This response has been attributed to fluorescence of the plexiglass structure or air. Photographs taken of the plexiglass structure during the AURORA radiation pulse indicate a bright fluorescence. This APD signal should be compared with HDL's pulse shape monitor of Figure 19 or the cable photocurrent shown in Figure 15B. In Figure 21 a photograph of the region where the NIL will occur is shown. The blurry glow is attributed to the plexiglass structure. The optical system was designed to relay the image of the 1 cm long NIL. However, an image with a smaller magnification will be relayed by the system if the parabolic mirror is ignored. Although thisimage is out of focus, it is sufficient to generate the blurry background on the photograph and the observed photodiode response. The signals observed on the current and voltage probes during shots where nuclear lightning was observed are several volts in amplitude. The noise signals observed on both AURORA and 100 kV background test shots are insignificant when compared to the observed signal levels.

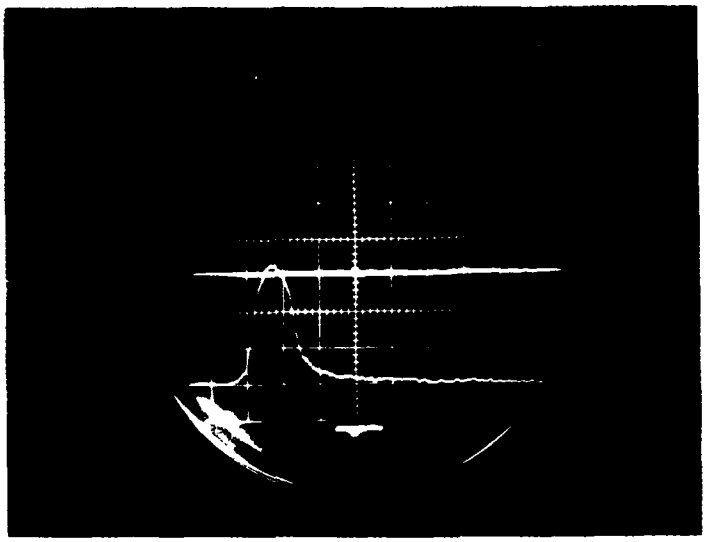

Upper trace: extra

Lower trace:
APD#1 50 mV/div

100 ns/div

Figure 20. APD response to AURORA without HV pulser.

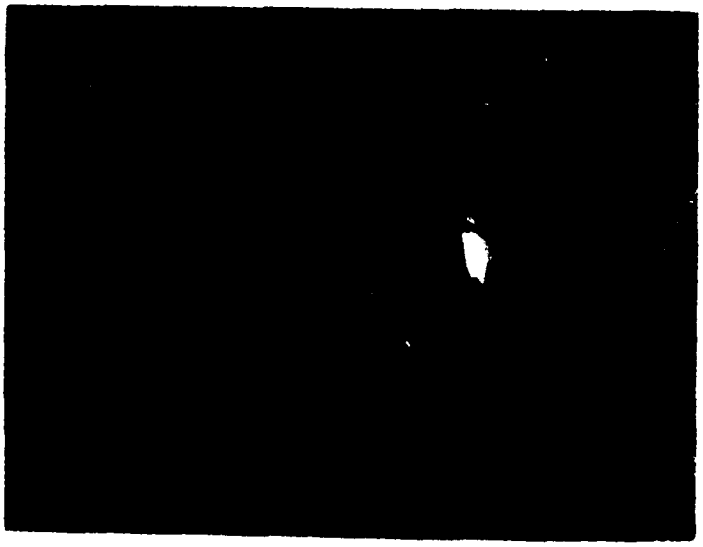

Figure 21. Plexiglass structure fluorescence as viewed by the optical system.

3.1.6 Pre-Test Shots Without AURORA

Table 3 is an annotated index of all test activities including several shots without the AURORA radiation pulse but with the 100 kV pulser. The cathode was placed close enough to the pin for arc-over to occur. When arc-over occured the pulser dumped all of its energy through the arc. This is shown in the current and voltage records in Figure 22. This arc was much brighter than the NIL event since it draws a larger current. Figure 23, the photodiode response, shows the photodiodes saturating immediately after the arc closes the gap. A photograph of the arc is shown in Figure 24. This photograph was taken with the aperture set at its smallest value. The wide band of light that appears to be in the background is an image of the arc. An image of the cathode grid and pin is also observed. This is due to the accidental (pin hole) imaging properties of the optical system discussed in Section 3.1.5. The cathode and pin apppear as a shadow in front of the arc because of the small aperture. These test shots verified that the optical system and the related electronics were operating properly.

3.2 NUCLEAR LIGHTNING RESULTS

To accomodate for the lower voltage available from the pulser during the AURORA radiation pulse, the separation between the cathode and the pin was reduced. This increased the electric field to encourage the creation of a nuclear discharge. Evidence of nuclear lightning was first observed at a pin-cathode spacing of 10 cm (5 shots). Arc-over occurred at a 5 cm spacing. An arc ≈0.5 cm long was observed at a spacing of 7.5 cm (two shots). Open shutter photographs of nuclear streamers observed at this spacing are shown in Figure 25A and B. While it is difficult to determine the diameter of this streamer it is clearly no greater than 1 mm. The response of four APD's to a nuclear streamer in shot 3715 (Figure 25B) is shown in Figure 26. APD number 4 is focused on the region at the tip of the pin. APD number 3 is focused on the next region, with APDs number 2 and 1

Table 3. Annotated table of experimental activities for the AURORA nuclear lightning test (set-up experiment 3/20-22/82)

Event 1.0	Date (1982)	Time	Trigger	Timing	Observations 1.0
P1	3/23 AURORA	—	50Q and	NA	Cathode to anode arc
P2		—	50Q only	NA	Cathode to anode arc
P3		—	50Q only	TAG 2	Cathode to anode arc
3700		1531	50Q and AURORA	1,2,3, μs early	HV cable breakdown
3/23/1		—	50Q only	NA	
3/23/2		—			
3/23/3		—			Create arc in test fixture, use for optical alignment and data acquisition adjustement
3/23/4		—			
3/23/5		—			
3/23/6		—			

Table 3 (continued)

Event 1.0	Date (1982)	Time	Trigger	Timing	Observations 1.0
3701		1156	50Q and AURORA	1.31 μs	{25 cm spacing/no streamers reversed 50Q polarity}
—		—	—	—	
3702		1402	50Q and AURORA	1.31 μs	25 cm spacing/no streamer
3703		1529	"	1.31 μs	" " " " "
3/23/8		—	50Q only	TAG2-1.2 ns	Small gap
3/23/9		—			" "
3704	3/24	0937	50Q + AURORA	*	*50Q = TAG2 - 1.38 μs Scopes = TAG2 - 1.1 μs No streamers
3705					
3706	3/24	1109	50Q + AURORA	50Q Scopes	TAG2 - 1.29 μs {no streamers} TAG2 - 1.09 μs
3707		1141	AURORA only no pulser	TAG2-1.28 μs	reduce gap to 10 cm located and eliminated noise sources

Table 3 (concluded)

Event 1.0	Date (1982)	Time	Trigger	Timing	Observations 1.0
3708		1323	500Q and AURORA	TAG2 - 1.29 μs TAG2 - 1.1 μs	observed small NIL
3709		1404	"	TAG2 - 1.33 μs	Arc-over
3710		1541	"	TAG2 - 1.3 μs	Small NIL
3711		1600		" "	Small NIL Added poly insulation
3712		—	"	None	Small NIL Reduce gap to 5 cm
3713		1758		TAG - 1.3 μs TAG - 1.09	breakdown across gap spread gap to 7.5 cm
3714		1	AURORA only 50Q shorted	"	Noise test
3715		1922	50Q AURORA	TAG - 1.29 μs TAG - 1.11 μs	Good NIL
3716		≈2000	50Q AURORA	None	Good NIL

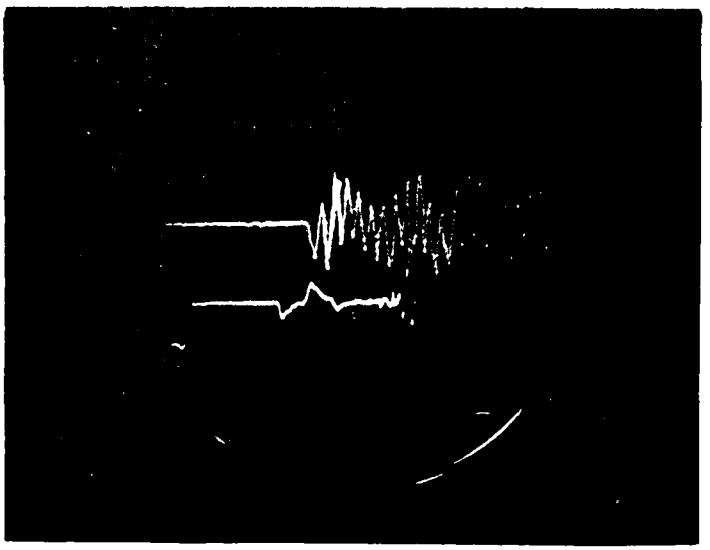

Upper trace: (enhanced)
voltage 78 kV/div

Lower trace: extra

200 ns/div

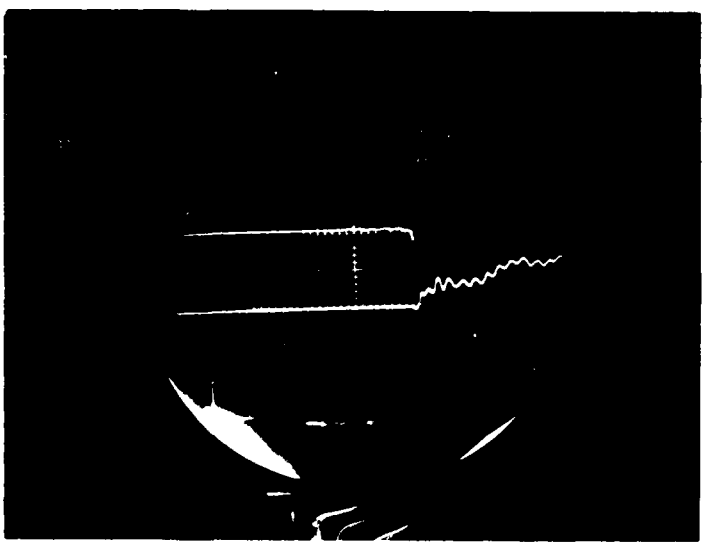

Upper trace: extra

Lower trace:
current 5.5 kA/div

100 ns/div

Figure 22. Voltage and current behavior with arc-over.

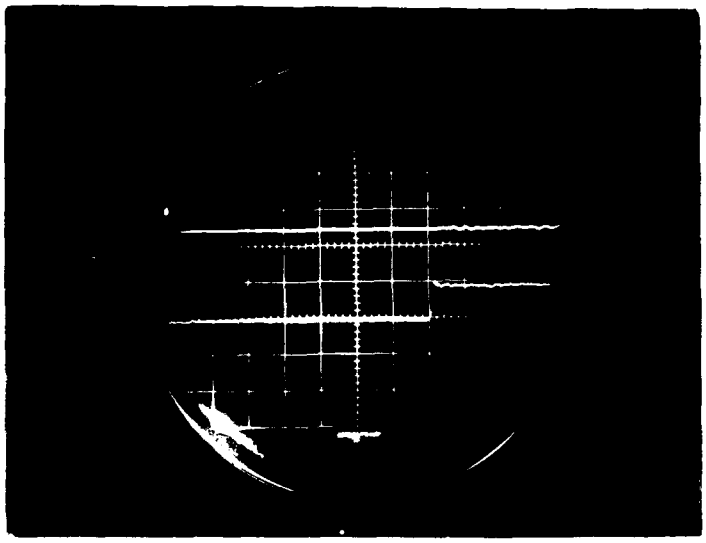

Upper trace: extra

Lower trace:
APD#1 500 mV/div

100 ns

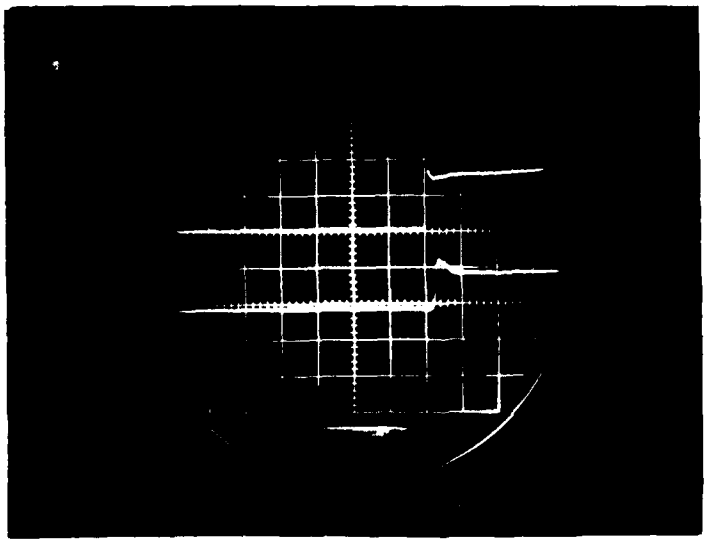

Upper trace:
APD#2 500 mV/div

Lower trace:
APD#3 500 mV/div

100 ns

Figure 23. APD response to arc-over.

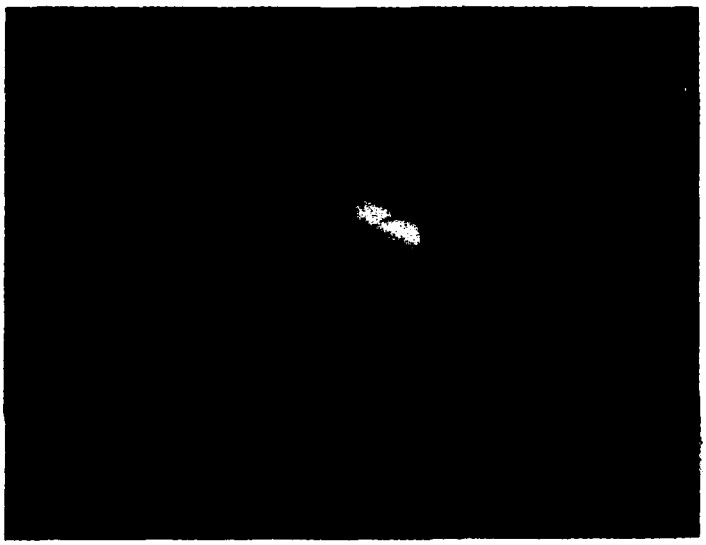

Figure 24. Photograph of arc-over.

Pin side

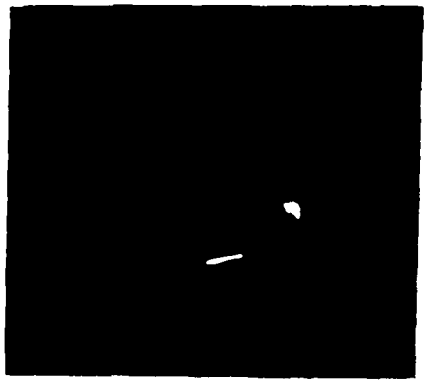

A. Shot 3716

Pin side

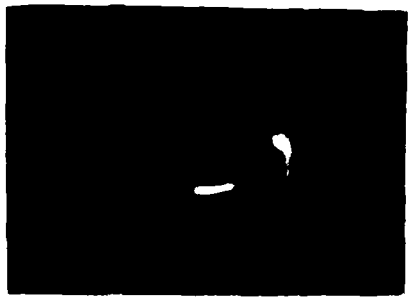

B. Shot 3715

Figure 25. Photographs of nuclear lightning arcs.

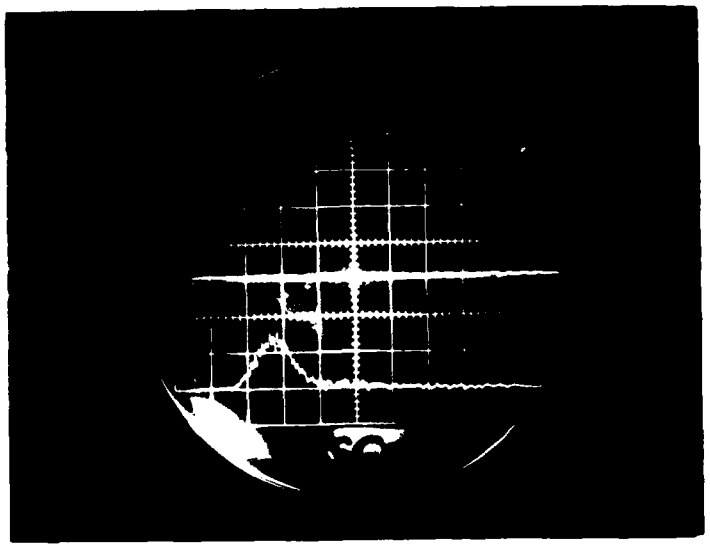

Upper trace: extra
Lower trace: APD#1 50 mV/div

100 ns/div

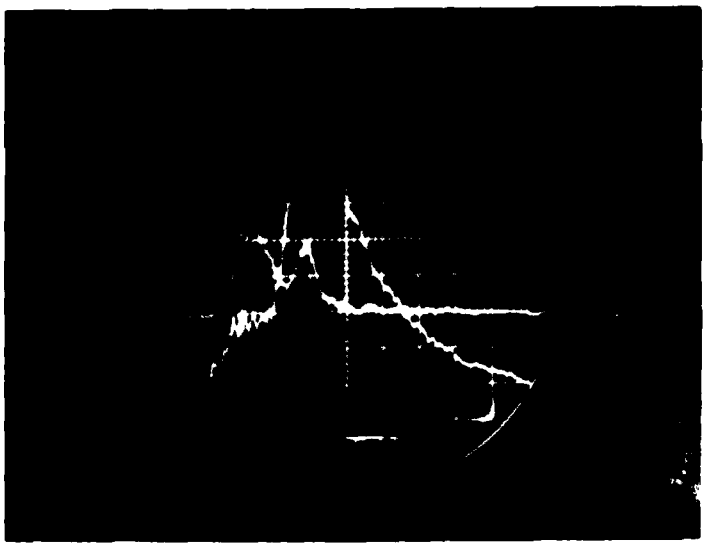

Upper trace: APD#2 50 mV/div (enhanced)
Lower trace: APD#3 50 mV/div (enhanced)

100 ns/div

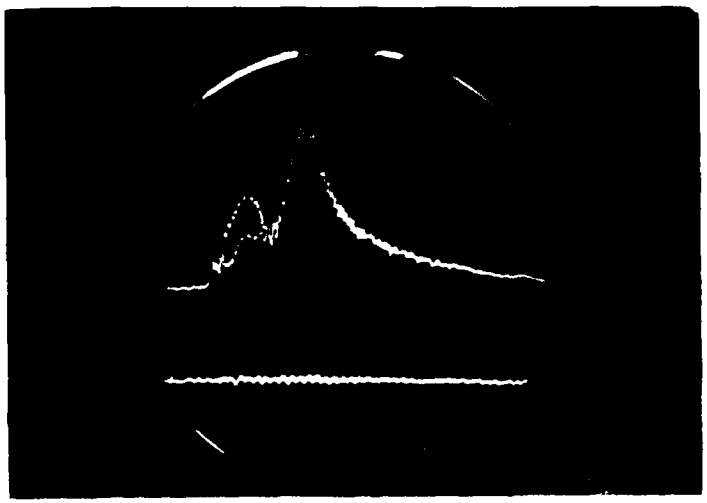

Upper trace: APD#4 100 mV/div (enhanced)
100 ns/div

Figure 26. APD response to nuclear arc.

focused on the following two regions. The field-of-view of each region is 0.25 cm long. The nuclear streamer appeared about 150 ns after onset of radiation. When the image of the NIL enters a region it is indicated by the signal departing from the bell shaped radiation signal. The streamer was observed by diodes 2-4, but never entered the field of view of diode 1. The onset of the radiation pulse (indicated by the fluorescence) was used as a fiducial mark to correlate the time on the traces.

The position of the tip of the NIL is plotted as a functon of time in Figure 27. Timing uncertainty is primarily related to our ability to distinguish the onset of the NIL signal in the scope photograph and is estimated to be ≈± 6 ns. The location uncertainty of the photodetector field of view with respect to the tip of the pin is estimated to be ± 0.13 cm. The field-of-view separations have no uncertainty since all detectors share a common optical path. In this investigation no streamer was ever long enough to enter the field-of-view of avalanche photodiode 1. The peak optical intensity typically occurred 175-260 ns after onset of radiation and voltage (or ≈25-110 ns after initiation of the streamer). The peak intensity approximately coincided with the cessation of radiation. That the streamer existed at these late times but was not seen by APD 1 is clear evidence that it stopped propagating before entering the field of view of detector 1. This observation helps confirm these were nuclear streamers which require conductive air rather than electrostatic air breakdown "arcs".

In Figure 28 the dose rate, the applied voltage, the pin current,- and the response of APD number 4 are plotted on the same time base (high frequency (≈1 GHz) noise has been filtered out of the APD data). Four times are highlighted. The application of high voltage was synchronized with the onset of radiation (t_0). Notice the applied voltage dropped as dose rate increased and recovered on cessation of radiation . The peak in the "fluorescence" signal coincides with the peak dose rate (t_2). The nuclear lightning streamer enters the APD field-of-view, or its intensity equals the

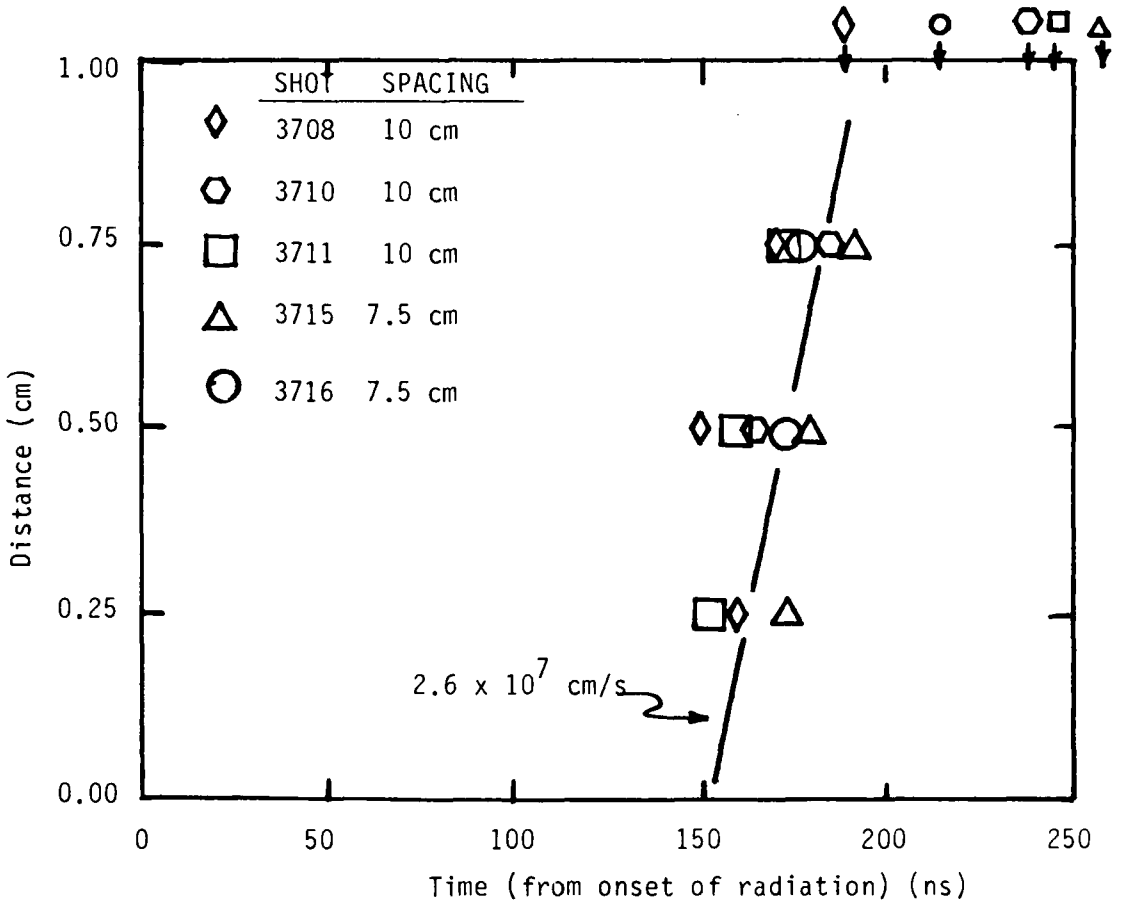

Figure 27. Location of tip of channel versus time. The line line does not represent a fit to the data, it merely represents a velocity the data may be compared to. Notice there seems to be an incubation time of about 150 ns between the application of stress and the observation of a streamer.

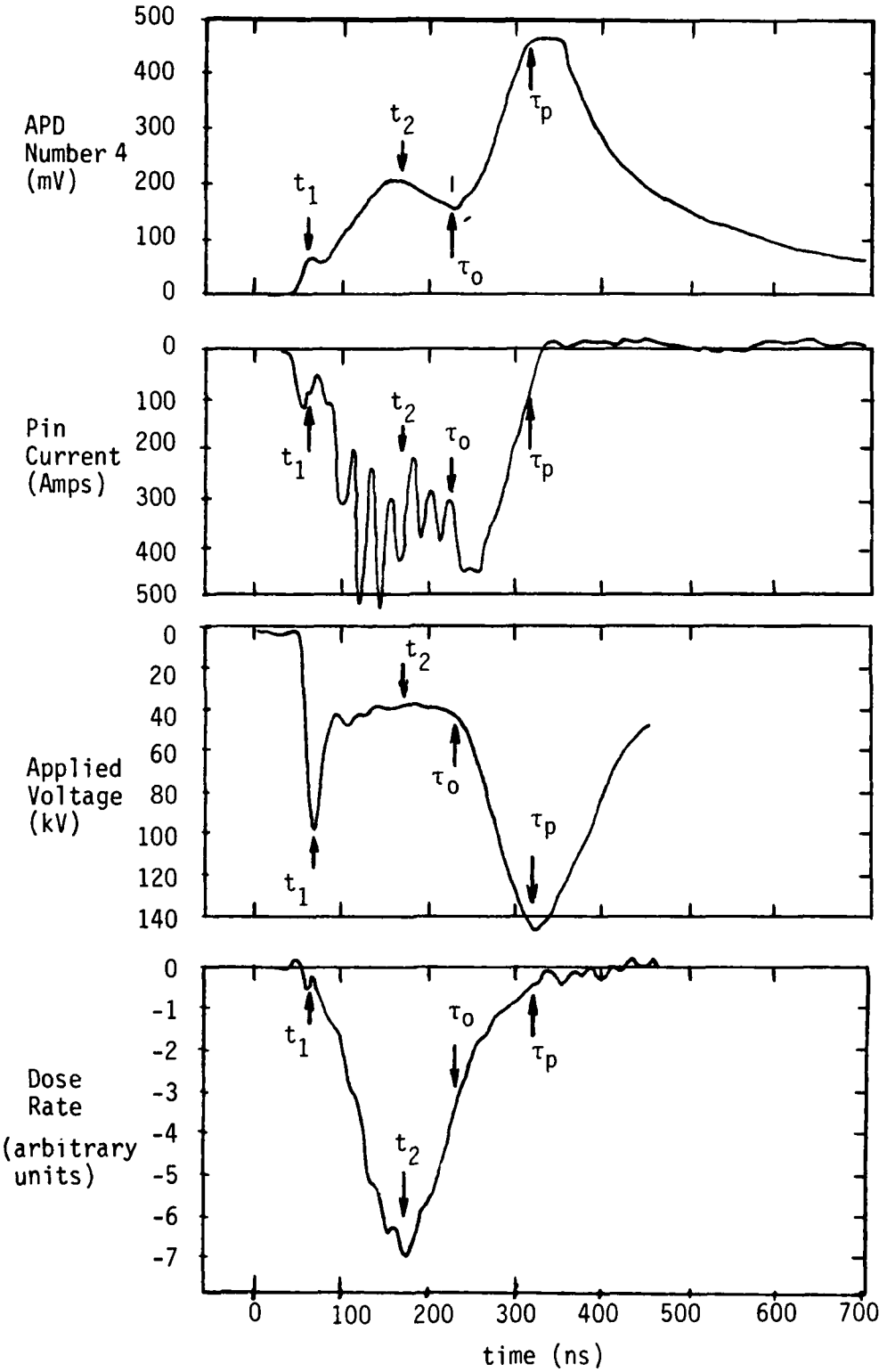

Figure 28. Diagnostics on Shot 3715.

fluorescent signal, at τ_o and reaches an intensity maximum at τ_p. Notice there is apparently an incubation time for the formation of a streamer. Dose rate and current are actually falling as the streamer intensity grows. Applied voltage grows as dose rate and current decrease. The peak intensity is thought to occur when the heating and cooling rates are equal. The current flowing through the streamer at this time is the self-sustaining current. The self-sustaining current appears to be less than 100 Amps. The slow decay of the intensity is related to the cooling rate. The applied voltage is increasing during the growth of the NIL. The diagnostics of this shot are very similar to those for other shots. The peak current on shots where nuclear streamer were observed ranges from 100 A to 440 A. The applied voltage at the peak of AURORA varied from ≈ 24 kV to ≈ 48 kV between the shots.

3.3 COMPARISON OF EXPERIMENTAL RESULTS WITH THEORY

The fact that dose rate current and voltage were all varying simultaneously during the streamer propagation make it difficult to compare the instantaneous velocity with expectations based on theory. The line drawn through the data points of Figure 27 is just for comparison and does not represent a true "fit" to the data.

In Reference 2, Frese, et al., did a preliminary estimate of the propagation theory of nucler lightning. In this oversimplified model they assumed the electric field was a constant E_a (the avalanche field) within a spherical shell of radius (R), so that the current density increased with decreasing radius (r) as r^{-2}. They further assumed the power $P = \int JE_a dA$, deposited in a spherical volume of radius (a) would adiabatically* heat the air contained therein. Calculations suggest only radiation losses can occur on these time scales. Expansion and conduction don't have time to move much energy. Assuming a constant channel diameter, which seems consistent both

* without energy loss mechanisms

with theory and observation for this short length, the streamer will grow longitudinally at a rate determined by the ratio of power deposited to heat (Q) required to thermally ionize the air. According to this model the velocity v is

$$v = \sigma_o E_a^2 R^2 / Qa \qquad (1)$$

where σ_o is the radiation induced conductivity of air, $\sigma_o \approx \dot{KD}$. Frese, et al., assumed Q = 40 J/cm^2 and deduced a = 0.025 cm by taking v = 1 x 10^7 cm/s from the Mike Shot NIL observations.

In this experiment we have direct measurements of the applied voltage, current and streamer displacement. Dose rate is easily and accurately derived from dosimetry. Air conductivity can be approximated from dose rate and published data. Unfortunately all these parameters vary rapidly over the 50 ns that the observed streamer propagated. However the displacement X of the channel tip can be estimated and compared with expectations. Alternatively we can treat Qa as an unknown and use these experimental data to derive Qa.

First, the total instantaneous power dissipated in the air cell is V(t)I(t). Solution of the electrostatic problem where E = E_a out to radius R and falls as r^{-2} there after results in $V(R) = V_{appl}/2$ (Ref. 4).

Therefore a channel of constant diameter can propagate no farther than

$$X(t) = \frac{1}{2\pi a^2 Q} \int_o^t V(t)\, I(t)\, dt \qquad (2)$$

in time t.

This is certainly an overestimate because:

1) The adiabatic approximation ignores all power loss mechanisms (i.e., radiation).

2) Most (90%) of the power actually flows through a cylinder surrounding the pin and/or channel, not just across a hemisphere surrounding the tip.

Another way to estimate the channel propagation from the available data ($V(t)$ and $\dot{D}(t)$) is by substituting for E_a and R in terms of the electrode potential of the experiment V, (the voltage at the surface of the avalanche region is V/2) (Ref. 4). For this case the position as a function of time is given by

$$X(t) = \frac{K}{4Qa} \int_o^t \dot{D}\, V^2\, dt \qquad (3)$$

where K is the constant relating dose rate $\dot{D}$ and air conductivity σ, $(K \approx K_o\ e\ \mu/a = 7 \times 10^{-15}\ (\Omega\ cm\ rad/s))^{-1}$.

Figure 29 shows $X(t)$ calculated from Equation 2 and 3 as well as the measured data for event #3715. For comparison purposes the data is plotted as it would appear if $Q = 40\ J/cm^3$ and $a = 0.025$ cm (values taken from Reference 2). It would appear that these data can be accomodated by adiabatic theory if Qa is considerably less than inferred from previous nuclear tests (i.e, Qa about .05 J/cm^2 rather than about 1 J/cm^2). We suppose that the channel diameter 2a of a 0.75 cm long streamer may be considerable smaller than the diameter of a 6×10^4 cm long streamer. The plot of Equation 2 indicates that the measured data is physically reasonable from an energy viewpoint.

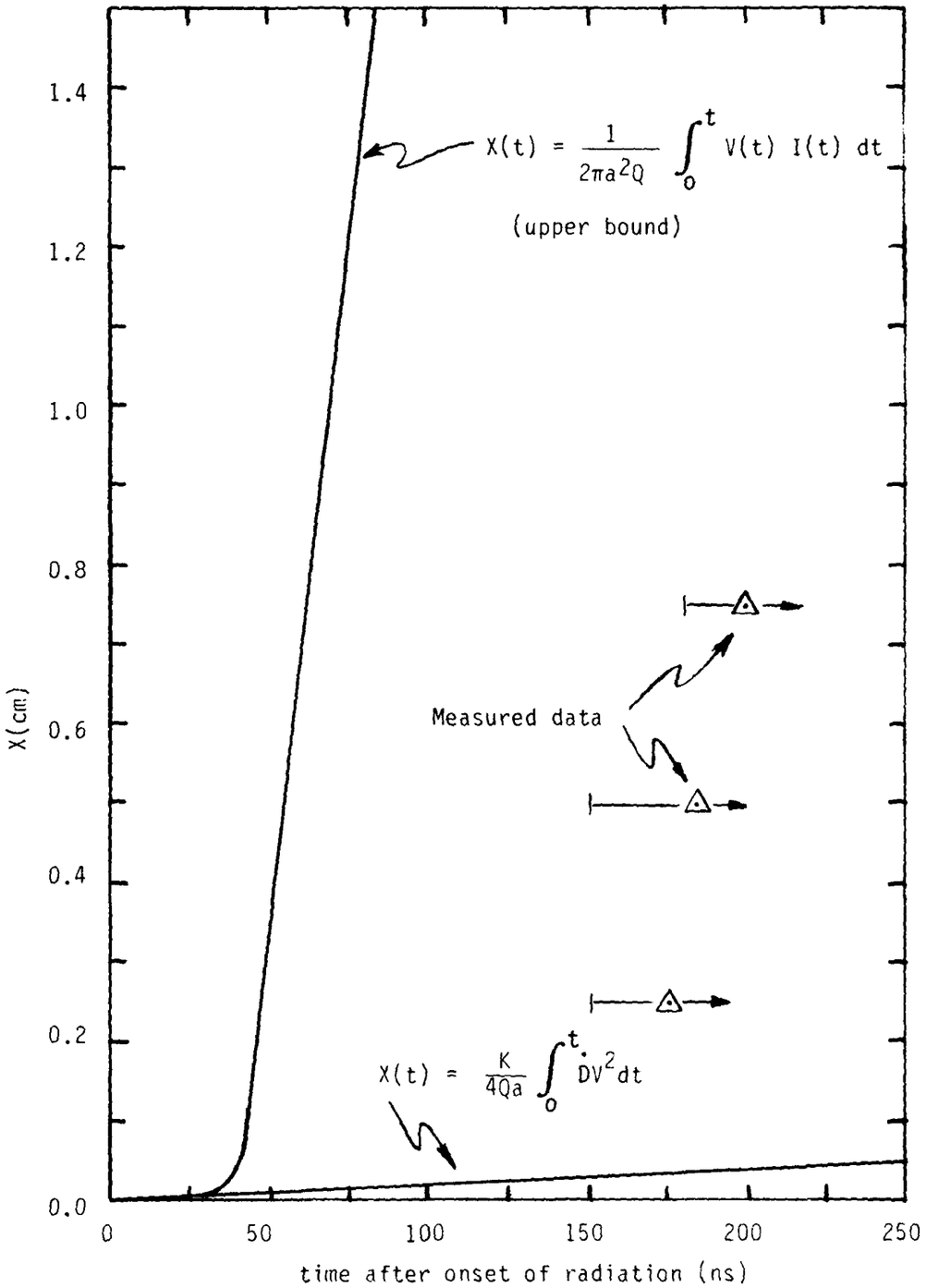

Figure 29. Comparison of data with two models.

The reason for the apparent (≈125-150 ns) incubation time suggested by these data is not known. It is conceivable that at early times when the tip is near the metal pin that the energy losses are larger than after the tip has moved away. Thus the Qa product is so initially large and hence the tip velocity so low that the tip remains under the cooling influence of the metal pin for roughly 125 ns (the tip velocity should be proportional to the difference between the heating and cooling rates).

SECTION 4
SUMMARY

This report describes an experiment designed to duplicate the conditions at the tip of nuclear lightning in a laboratory environment by scaling dose rate up and dimensions down. All indications are that the experiment produced miniature nuclear lightning bolts (about 0.75 cm long) at least 5 times in an AURORA exposure. These events were photographed, electrically characterized and the discharge propagation was measured. Agreement with expectations based on previous atmospheric test observations and theory is judged to be reasonable. This experiment lends considerable credibility to the propagation theory of nuclear induced lightning.

There remain some uncertainties, in the theory of nuclear lightning particularly in the general areas of air chemistry (i.e., species and reaction rates) and radiative transfer. That nuclear lightning can be created in laboratory conditions has been demonstrated. Experiments such as time resolved spectroscopy designed to reduce the remaining questions should be considered.

REFERENCES

1. M.A. Uman, D.R. Seacord, G.H. Price and E.T. Pierce, "Lightning Induced by Thermonuclear Detonations", Journal Geophysical Research II, 1591 (1972).

2. M.H. Frese, J.L. Gilbert, and C.L. Longmire, "Nuclear Lightning, I. Currents Carried by the Discharge," Mission Research Corporation, Albuquerque, NM AMRC-R-239, September 1980.

3. Ropbert Gardner, Conrad Longmire, James L. Gilbert, Michael H. Frese, "Nuclear Lightning VII Growth Rate of Discharge, AFWL-TR-81-192 (V2) February 1982.

4. Joe Chervenak, "Laboratory Simulation of Nuclear Lightning", MRC/SD-N-76, 18 November 1981.

5. V.van Lint and J.W. Erler, "Buried Conductor Studies," Mission Research Corporation, MRC/SD-R-93, December 1981, p.214.

6. R.D. Hudson, Jr. Infrared System Engineering, Wiley-Interscience, John Wiley and Sons, New York, 1969, pg. 83.

7. Robert L. Gardner, personal communication.

APPENDIX

ELECTRIC FIELD MEASUREMENT (LANGMUIRE PROBE)

The boundary layer voltage is measured by placing a grid ≈ 2 cm below the cathode. The grid is made of 4 mil wire spaced 1 cm apart. The grid can best be described in this case as a Langmuire probe. As electrons pass through the grid, some electrons will strike the grid and charge it up until the voltage is slightly larger than the ambient electric potential, then the incident electrons will be deflected from the grid. Loeb (Ref. A1) shows that this votage increase is given by

$$V_W = \frac{kT_-}{2e} \ln \frac{T_- M_+}{T+M_-}$$

Where M_+ is the atomic mass of positive ions, M_- is the atomic mass of the electrons, T_- and T_+ are the temperature of the electrons and the ions, respectively. k is boltzmann's constant and e is the electro charge. T_- for ≈ 1 eV electrons is 11.6×10^{3}° K, T_+ for N_2-O_2 ions is ≈ 300° K, M_- is 5.5×10^{-4} AMU for electrons, M_+ for N_2 and /or O_2 is ≈ 60 AMU, e is 1.6×10^{-19} coul and k is 1.38×10^{-23} J/mole° K. For this case V_W is ≈8 volts. This is insignificant relative to the 90 kV being measured.

The entire grid is 10 cm in diameter. The percent of the current available to the grid is proportional to the area subtended by the grid, shown by

$$\% \text{ of current on grid} = \frac{\text{cross sectional area of grid wire}}{\text{total area subtended by the grid}} \times 100$$

A1. L.B. Loeb, Basic Processes of Gaseous Electronics, University of California Press, Berkeley, California, 1955, p.337.

For the grid described above, the area of the wire is 1.72×10^{-4} m^2, and the total area is 7.85×10^{-3} m^2, resulting in 2% of the total current picked up by the grid. Most of the current flowing to the pin will also flow through the grid.

Currents ranging fom 100 to 1,000 Amps were expected at the pin. Grid currents between 2 and 20 amps were expected. The voltage probe used to monitor the grid could not draw more than the grid current, or the grid voltage would drop below the value of the ambient field potential near the grid. The voltageon the grid was measured with a ≈ 28 kΩ voltage divider. The signal was carried to the divider via an insulated cable placed approximately along an equipotential. The voltage divider consisted of 20, 1.4 kΩ resistors and one 1.8 Ω measurement resistor. The response of the divider was calculated from

$$V_{OUT} = V_{IN} \frac{R_L}{R_L + R_D}$$

where R_L (load resistor) is 1.8 Ω and R_D (divider resistor) is 28 kΩ. $V_{OUT}/V_{IN} = 6.4 \times 10^{-5}$. For a grid voltage of ≈ 90 kV, the output voltage 5.8 V and the current drawn amps response time of this probe was given by (Ref. 5)

$$\tau_p = \frac{N^2 R_s C_s}{\pi^2}$$

where N (number of resistors) was 20, R_s (resistor value) was 1.4 kΩ and C_s (shunt capacitance per resistor) was ≈ 0.5 pF. For this probe τ_p = 28 ns. The voltage across the 1.8 Ω resistor was sent via an RG-58 (50 Ω) coaxial cable to the data room . The grid and voltage probe are shown in Figure A1.

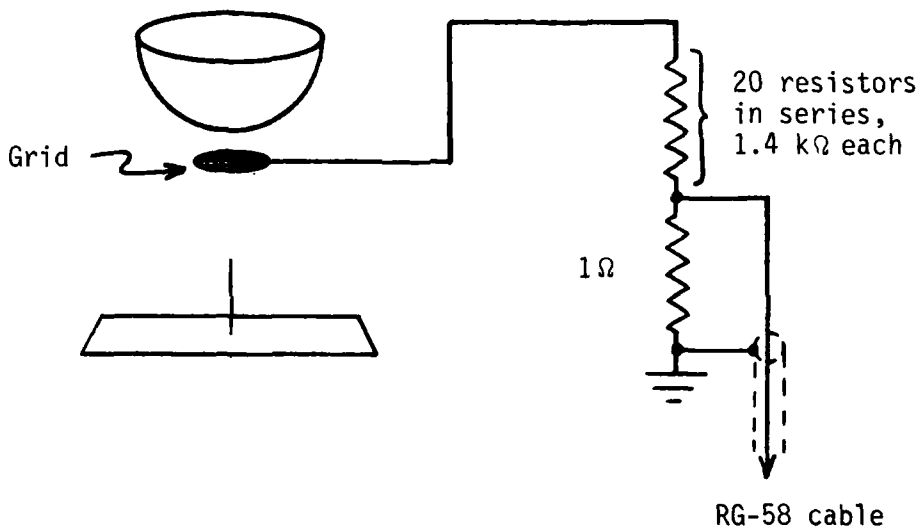

Figure A1. Grid placement and voltage sensor.

DISTRIBUTION LIST

DEPARTMENT OF DEFENSE

Assistant to the Secretary of Defense
Atomic Energy
ATTN: Mil Appl
ATTN: Exec Assistant

Defense Communications Agcy
ATTN: Code 312
ATTN: Code C313

Defense Communications Engr Ctr
ATTN: Code R123
ATTN: Code R400
ATTN: Code R720, C. Stansberry

Defense Intelligence Agcy
ATTN: RTS-2A
ATTN: DB-4C2, D. Spohn

Defense Nuclear Agcy
ATTN: NATA
ATTN: STNA
2 cy ATTN: RAEE
4 cy ATTN: TITL
4 cy ATTN: DDST, V. van Lint

Defense Technical Info Ctr
12 cy ATTN: DD

Field Command Defense Nuclear Agcy
Det 1
Lawrence Livermore Lab
ATTN: FC-1

Field Command
Defense Nuclear Agcy
ATTN: FCLMC, H. Putnam
ATTN: FCPR
ATTN: FCTXE
ATTN: FCTT
ATTN: FCTT, W. Summa
ATTN: FCTT, G. Ganong

Interservice Nuclear Wpns School
ATTN: TTV

Joint Chiefs of Staff
ATTN: J-3

Joint Strat Tgt Planning Staff
ATTN: NRI-STINFO Library
ATTN: JLA, Threat Appl Div
ATTN: JPST
ATTN: JSAS

National Communications System
ATTN: NCS-TS

National Security Agcy
ATTN: R-52, O. van Gunten
ATTN: TDL
ATTN: S-232, D. Vincent

Under Secretary of Defense for Rsch & Engrg
ATTN: Strat & Space Sys (OS)

DEPARTMENT OF THE ARMY

BMD Systems Cmd
ATTN: BMDSC-AOLIB
ATTN: BMDSC-HLE, R. Webb

Deputy Chief of Staff for Rsch Dev & Acq
ATTN: DAMA-N-CSS, N. Barron

Electronics Tech & Devices Lab
ATTN: DELSD-L, W. Werk

Fort Huachuca
ATTN: CCH-PCA-TR

Harry Diamond Labs
ATTN: DELHD-TD
ATTN: DELHD-NW-P
ATTN: DELHD-TF
ATTN: DELHD-TA-L
ATTN: DELHD-NW-EC
ATTN: DELHD-NW-EA
ATTN: DELHD-NW-EE
ATTN: 00100 Cmdr/Tech Dir/Div Dir
ATTN: DELHD-NW-EB
ATTN: DELHD-NW-ED
ATTN: DELHD-NW-E
ATTN: DELHD-R
ATTN: NWPO
ATTN: DELHD-NW, J. Bombardt
2 cy ATTN: DELHD-NW-RC

Research & Dev Ctr
ATTN: DRDCO-SEI
ATTN: DRCPM-ATC

US Army Armor Ctr
ATTN: Tech Library

US Army Ballistic Rsch Labs
ATTN: DRDAR-BLE
ATTN: DRDAR-BLB, W. Vanantwerp

US Army Comm-Elec Engrg Instal Agcy
ATTN: CCC-CED-SES

US Army Communications Cmd
ATTN: ATSI-CD-MD
ATTN: CC-OPS-PD
ATTN: CC-OPS-OS
ATTN: CC-LOG-LEO

US Army Communications Sys Agcy
ATTN: CCM-AD-SV
ATTN: CCM-RD-T

US Army Engr Div Huntsville
ATTN: HNDED-SR

US Army Intel Threat Analysis Det
ATTN: Admin Officer

US Army Intel & Sec Cmd
ATTN: Tech Library
ATTN: Tech Info Fac

DEPARTMENT OF THE ARMY (Continued)

US Army Materiel Sys Analysis Actvy
ATTN: DRXSY-PO

US Army Nuclear & Chemical Agcy
ATTN: MONA-WE

US Army Test and Evaluation Cmd
ATTN: DRSTE-EL
ATTN: DRSTE-FA

US Army Training & Doctrine Cmd
ATTN: ATCD-Z

US Army White Sands Missile Range
ATTN: STEWS-TE-AN, J. Okuma

USA Missile Cmd
ATTN: DRCPM-PE-EG, W. Johnson
ATTN: DRSMI-SF, H. Henriksen
ATTN: Doc Sec
ATTN: DRCPM-PE-EA, W. Wagner

DEPARTMENT OF THE NAVY

Naval Air Systems Cmd
ATTN: AIR 350F

Naval Electronic Systems Cmd
ATTN: PME 117-21

Naval Ocean Systems Ctr
ATTN: Code 08, J. Rockway
ATTN: Code 54, C. Fletcher
ATTN: Code 7309, R. Greenwell
ATTN: Code 8123, S. Lichtman

Naval Ordnance Station
ATTN: Standardization Div

Naval Postgraduate School
ATTN: Code 1424 Library

Naval Research Lab
ATTN: I. Vitkovitsky
ATTN: Code 6623, R. Statler
ATTN: Code 6750
ATTN: Code 2627, D. Folen
ATTN: Code 2000, J. Brown
ATTN: Code 1434, E. Brancato

Naval Surface Wpns Ctr
ATTN: Code F30
ATTN: Code F32, E. Rathbun

Naval Surface Wpns Ctr
ATTN: Code F-56

Naval Wpns Ctr
ATTN: Code 343 (FKA6A2) Tech Svcs

Naval Wpns Eval Fac
ATTN: Code AT-6

Naval Wpns Spt Ctr
ATTN: Code 11E

Office of the Deputy Chief of Naval Ops
ATTN: OP 981N1

DEPARTMENT OF THE NAVY (Continued)

Office of Naval Research
ATTN: Code 427

Strategic Systems Project Office
ATTN: NSP-2342, R. Coleman
ATTN: NSP-230, D. Gold
ATTN: NSP-43
ATTN: NSP-27334
ATTN: NSP-2701, J. Pitsenberger

DEPARTMENT OF THE AIR FORCE

Aeronautical Systems Div
ATTN: ASD/YYEF
ATTN: ASD/ENFTV

Aerospace Defense Cmd
ATTN: DEE

Air Force Aeronautical Sys Div
ATTN: ASD/ENAMA, J. Corbin

Air Force Weapons Lab
ATTN: NTYEE, C. Baum
ATTN: NTYC, M. Schneider
ATTN: CA
ATTN: NXS
ATTN: NTYEP, W. Page
ATTN: NT
ATTN: SUL
ATTN: NTN

Air Logistics Cmd
ATTN: OO-ALC/MM
ATTN: OO-ALC/MMEDO, L. Kidman
ATTN: OO-ALC/MMETH, P. Berthel

Air University Library
ATTN: AUL-LSE

Ballistic Missile Office
ATTN: ENSN, W. Wilson
ATTN: M. Stapanian
ATTN: ENSN, W. Clark

Deputy Chief of Staff
Research, Development, & Acq
ATTN: AFRDQI

Electronic Systems Div
ATTN: SCS-1E

Foreign Tech Div
ATTN: TQTD, B. Ballard
ATTN: NIIS Library

North American Air Defense Cmd
ATTN: NORAD/J5YX

Rome Air Development Ctr
ATTN: TSLD

Sacramento Air Logistics Ctr
ATTN: MMSREM, F. Spear
ATTN: MMCREB, F. Schrader
ATTN: MMIRA, J. Demes

Space Div
ATTN: IND

DEPARTMENT OF THE AIR FORCE (Continued)

Space Div
ATTN: YLXT

Strategic Air Cmd
ATTN: NRI-STINFO Library
ATTN: DEL
ATTN: NRI, G. Matzke
ATTN: XPFS, G. Skluzacek

DEPARTMENT OF ENERGY

Department of Energy
ATTN: WSSB
ATTN: CTID

Emergency Electric Power Adm
US Department of Energy
ATTN: L. O'Neill

OTHER GOVERNMENT

Central Intelligence Agency
ATTN: OSWR/NED

Department of Transportation
Federal Aviation Admin
ATTN: Sec Div ASE-300

Federal Emergency Management Agcy
ATTN: SL-EM, J. Hain

Federal Preparedness Agcy
General Services Admin
ATTN: ESTE, M. Murtha

DEPARTMENT OF ENERGY CONTRACTORS

University of California
Lawrence Livermore National Lab
ATTN: Tech Info Dept Library
ATTN: L-96, T. Donich, Class L-94
ATTN: L-156, H. Cabayan
ATTN: L-153, D. Meeker, Class L-477
ATTN: L-10, H. Kruger, Class L-94
ATTN: L-156, E. Miller

Los Alamos National Lab
ATTN: MS 670, J. Hopkins
ATTN: MS 670, J. Malik
ATTN: B. Noel
ATTN: MS 668, J. Malik
ATTN: C. Benton

Sandia National Lab
ATTN: T. Martin
ATTN: C. Vittitoe
ATTN: R. Parker
ATTN: ORG 9336, E. Hartman
ATTN: G. Yonas

DEPARTMENT OF DEFENSE CONTRACTORS

Aerospace Corp
ATTN: J. Reinheimer
ATTN: C. Pearlston
ATTN: I. Garfunkel
ATTN: C. Greenhow
ATTN: R. Crolius
ATTN: Library

DEPARTMENT OF DEFENSE CONTRACTORS (Continued)

Agbabian Assoc
ATTN: Library

AVCO Systems Div
ATTN: Library A830

Battelle Memorial Institute
ATTN: E. Leach

BDM Corp
ATTN: Corp Library

BDM Corp
ATTN: Library

Bendix Corp
ATTN: Doc Con

Bendix Corp
ATTN: M. Frank

Bendix Corp
ATTN: Dept 6401

Boeing Co
ATTN: Kent Tech Library
ATTN: D. Kemle
ATTN: H. Wicklein
ATTN: B. Hanrahan

Boeing Military Airplane Co
ATTN: C. Sutter

Booz, Allen and Hamilton, Inc
ATTN: Tech Library
ATTN: R. Chrisner

Calspan Corp
ATTN: Library

Charles Stark Draper Lab, Inc
ATTN: TIC MS 74
ATTN: K. Fertig

Cincinnati Electronics Corp
ATTN: L. Hammond

Computer Sciences Corp
ATTN: A. Schiff

Dikewood
ATTN: Tech Library for C. Jones
ATTN: Tech Library
ATTN: Tech Library for L. Davis

Dikewood Corp
ATTN: K. Lee

E-Systems, Inc
ATTN: J. Moore

Eaton Corp
ATTN: E. Karpen

EG&G Wash Analytical Svcs Ctr, Inc
ATTN: C. Giles

Electro-Magnetic Appl, Inc
ATTN: D. Merewether

DEPARTMENT OF DEFENSE CONTRACTORS (Continued)

Ford Aerospace & Communications Corp
ATTN: K. Attinger
ATTN: E. Poncelet, Jr

Franklin Institute
ATTN: R. Thompson

General Dynamics Corp
ATTN: Research Library

General Dynamics Corp
ATTN: Research Library

General Electric Co
ATTN: J. Andrews
ATTN: D. Nepveux
ATTN: J. Peden

General Electric Co
ATTN: C. Hewison

General Electric Co
ATTN: Tech Library

General Research Corp
ATTN: Tech Info Acq, S. Clow
3 cy ATTN: Tech Info Office

Georgia Institute of Technology
ATTN: Res & Sec Coord for H. Denny

Grumman Aerospace Corp
ATTN: L-01 35

Harris Corp
ATTN: A. Strain
ATTN: V. Pres & Mgr Prgms Div

Hazeltine Corp
ATTN: J. Okrent

Honeywell, Inc
ATTN: S&RC Library
ATTN: R. Johnson

Honeywell, Inc
ATTN: S. Graff
ATTN: W. Stewart

Horizons Technology, Inc
ATTN: R. Kruger

Hughes Aircraft Co
ATTN: CTDC 6/E110
ATTN: K. Walker

Hughes Aircraft Co
ATTN: A. Narevsky S32/C332

Hughes Aircraft Co
ATTN: K. Downing, MLS 100

IIT Research Institute
ATTN: ACOAT

IIT Research Institute
ATTN: I. Mindel
ATTN: J. Bridges

DEPARTMENT OF DEFENSE CONTRACTORS (Continued)

Institute for Defense Analyses
ATTN: Tech Info Svcs

International Tel & Tel Corp
ATTN: A. Richardson
ATTN: Tech Library

Ion Physics Corp
ATTN: H. Milde
ATTN: R. Evans

IRT Corp
ATTN: N. Rudie
ATTN: B. Williams

JAYCOR
ATTN: D. Higgins
ATTN: W. Hobbs
ATTN: W. Radaski

JAYCOR
ATTN: E. Wenaas
ATTN: R. Stahl

JAYCOR
ATTN: Library

Kaman Sciences Corp
ATTN: W. Rich
ATTN: A. Bridges
ATTN: F. Shelton
ATTN: N. Beauchamp

Kaman Tempo
ATTN: W. McNamara
ATTN: DASIAC
ATTN: R. Rutherford

Litton Systems, Inc
ATTN: MS 64-61, E. Eustis

Litton Systems, Inc
ATTN: J. Skaggs

Lockheed Missiles & Space Co, Inc
ATTN: Tech Info Ctr

Lockheed Missiles & Space Co, Inc
ATTN: B. Kimura
ATTN: S. Taimuty
ATTN: D. Nishida
ATTN: H. Thayn
ATTN: L. Rossi
ATTN: G. Heath

Lutech, Inc
ATTN: F. Tesche

Martin Marietta Corp
2 cy ATTN: M. Griffith

Martin Marietta Denver Aerospace
ATTN: D-6074, G. Freyer

McDonnell Douglas Corp
ATTN: T. Ender, 33/6/618

DEPARTMENT OF DEFENSE CONTRACTORS (Continued)

McDonnell Douglas Corp
ATTN: S. Schneider
ATTN: Tech Library Svcs

McDonnell Douglas Corp
ATTN: M. Potter
ATTN: W. McCloud, MS/36-49

Mission Research Corp
ATTN: EMP Group
ATTN: W. Crevier
2 cy ATTN: C. Longmire
5 cy ATTN: Doc Con

Mission Research Corp
ATTN: A. Chodorow
ATTN: L. McCormick

Mission Research Corp
4 cy ATTN: B. Passenheim
4 cy ATTN: J. Erler
4 cy ATTN: W. Vulliet

Mission Research Corp
ATTN: W. Ware
ATTN: J. Lubell
ATTN: W. Stark

Mitre Corp
ATTN: M. Fitzgerald

Norden Systems, Inc
ATTN: D. Longo
ATTN: Tech Library

Northrop Corp
ATTN: Rad Effects Gp
ATTN: B. Ahlport

Pacific-Sierra Research Corp
ATTN: L. Schlessinger
ATTN: H. Brode, Chairman SAGE

Palisades Inst for Rsch Svcs, Inc
ATTN: Records Supvr

Physics International Co
ATTN: Doc Con

R&D Associates
ATTN: M. Grover
ATTN: C. Mo
ATTN: Doc Con
ATTN: W. Graham
ATTN: W. Karzas

Rand Corp
ATTN: LIB-D
ATTN: W. Sollfrey

Raytheon Co
ATTN: G. Joshi

Raytheon Co
ATTN: H. Flescher
ATTN: M. Nucefora

DEPARTMENT OF DEFENSE CONTRACTORS (Continued)

Rockwell International Corp
ATTN: J. Erb
ATTN: N. Rudie
ATTN: V. Michel
ATTN: D/243-068, 031-CA31

Rockwell International Corp
ATTN: B. White

Rockwell International Corp
ATTN: F. Shaw

Rockwell International Corp
ATTN: B-1 Div TIC (BA0B)

S-CUBED
ATTN: A. Wilson

Sanders Assoc, Inc
ATTN: R. Despathy

Science & Engrg Assoc, Inc
ATTN: V. Jones

Science Applications, Inc
ATTN: N. Byrn

Science Applications, Inc
ATTN: W. Chadsey

Singer Co
ATTN: Tech Info Ctr

Sperry Corp
ATTN: M. Cort

Sperry Flight Systems
ATTN: D. Schow

Sperry Rand Corp
ATTN: Tech Library

SRI International
ATTN: A. Whitson
ATTN: E. Vance

Sylvania Systems Gp
ATTN: C. Thornhill
ATTN: L. Blaisdell

Sylvania Systems Gp
ATTN: D. Flood
ATTN: C. Ramsbottom

Sylvania Systems Gp
ATTN: J. Waldron
ATTN: A. Novenski
ATTN: J. Concordia
ATTN: I. Kohlberg

Teledyne Brown Engrg
ATTN: F. Leopard
ATTN: J. Whitt

Transient Limited Corp
ATTN: D. Clark

DEPARTMENT OF DEFENSE CONTRACTORS (Continued)

TRW Electronics & Defense Sector
ATTN: W. Gargaro
ATTN: O. Adams
ATTN: L. Magnolia
ATTN: R. Plebuch
ATTN: H. Holloway

United Technologies Corp
ATTN: Chief Elec Design

Varian Associates, Inc
ATTN: H. Jory

DEPARTMENT OF DEFENSE CONTRACTORS (Continued)

RCA Corp
ATTN: D. O'Connor
ATTN: L. Minich

Texas Instruments, Inc
ATTN: D. Manus
ATTN: Tech Library

TRW Electronics & Defense Sector
ATTN: R. Mortensen
ATTN: R. Kitter